ARMY RESEARCH LABORATORY

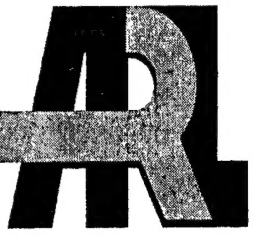

CYCLOPS, a Breakthrough Code to Predict Solid-Propellant Burning Rates

by Martin S. Miller and William R. Anderson

ARL-TR-2910 February 2003

NOTICES

Disclaimers

The findings in this report are not to be construed as an official Department of the Army position unless so designated by other authorized documents.

Citation of manufacturer's or trade names does not constitute an official endorsement or approval of the use thereof.

Destroy this report when it is no longer needed. Do not return it to the originator.

Army Research Laboratory
Aberdeen Proving Ground, MD 21005-5066

ARL-TR-2910 **February 2003**

CYCLOPS, a Breakthrough Code to Predict Solid-Propellant Burning Rates

Martin S. Miller and William R. Anderson
Weapons and Materials Research Directorate, ARL

Contents

List of Figures

List of Tables

1. Introduction

The trial-and-error approach has always played a central role in the development of new energetic materials for use as explosives and propellants. It is an approach dictated by necessity, not by choice. Final service acceptance of a new propellant has historically required extensive small and large-scale testing involving enormous monetary resources, lengthy development times, and the generation of great amounts of hazardous waste both in the manufacture of failed formulations and in their disposal. These burdens have been exacerbated over the last few decades by a number of other factors. The increasing sophistication of weapons systems has meant that their overall cost has grown far beyond that of the raw energetic materials that they utilize. Moreover, the escalating level of performance of these weapons systems has resulted in diminishing margins for error with regard to their proper functioning and safe operation. Finally, even further compounding these problems, is the galloping pace of change; timeliness in fielding an effective response to a new threat may well mean the difference between victory and defeat. The combination of these new fiscal, temporal, environmental, and safety constraints make it imperative that future propellant-development programs, such as that planned for the Future Combat Systems, reduce their reliance on the inefficient and wasteful trial-and-error method. The most rational way to accomplish this goal is through the development of smart computational design tools derived from a sound scientific understanding of propellant combustion.[1]

Unfortunately, in the field of propellant combustion, nature has given up her secrets most grudgingly. In part, this is due to the extremely hostile environment that propellants generate. In large guns, for example, action times range from a few tens of milliseconds for tank cannon to a few hundreds of milliseconds for an artillery piece. In this short time, the solid propellant is transformed from a metastable state at ambient temperature to equilibrium products at several thousands of Kelvins and pressures up to 7000 atmospheres. The reaction zone critical to determining the burning rate extends a mere hundred microns from the surface even at 10 atm and diminishes at higher pressures. Spatial temperature gradients at the burning surface are of the order of 10,000 K/cm at 10 atm and increase at higher pressures. Conducting controlled experiments under any one of these harsh circumstances of eye-blink times, hair-width distances, refractory temperatures, and crushing pressures presents a considerable experimental challenge, but the simultaneous presence of all four creates almost insuperable obstacles. Compounding the other experimental difficulties, even under constant-pressure conditions, propellant flames are flickering by nature. In addition to such macro-scale difficulties, the underlying mechanism of propellant combustion involves significant condensed-phase reactions and hundreds of gas-phase reactions among many dozens of species. The rates of most of these reactions are sensitive to both temperature and pressure. The result is an impressive tangle of physical and chemical phenomena.

Notwithstanding all the difficulties, progress in the basic science of propellant combustion has been achieved over the last dozen years. The major gas-phase chemical species and some radicals have been measured in flames of a number of burning energetic materials and propellants. Computational models have been developed which treat, with a high degree of rigor, the gas-phase processes, including reactions, convection, molecular diffusion, and thermal conduction. The condensed-phase treatment in these models is limited, not (so far) by computational insufficiency, but by the lack of definitive experiments revealing the detailed nature of the physical and chemical processes occurring there. A number of credible gas-phase reaction mechanisms have been assembled appropriate to several energetic compounds, and while some details of these mechanisms still require further study, the greatest speculation embodied in the models, by far, is in the detailed description of the condensed phases. While reliable experimental and theoretical methods are well established to refine our understanding of the gas-phase processes, such is not the case for the condensed phase. Unfortunately, owing to nearly intractable experimental and computational difficulties, this condition is not likely to be remedied in the near future.

To overcome this impasse, we recently proposed a hybrid approach[2] in which the conversion of condensed-phase material to gas is described by a semi-empirical relation, known in the propellant literature as a pyrolysis law, and the gas-phase processes of reactions and transport are described in elementary-reaction detail with considerable rigor. In this report we shall extend this approach to include multi-ingredient propellants and illustrate its promise through application of the model to several actual gun propellants. Our calculations of burning rate for real nitrate-ester-base propellants, including the complex ingredient nitrocellulose, are the first to be based on elementary reactions in the gas phase. It is expected that the proposed model will be useful for other classes of ingredients as well. In fact, we believe that the hybrid-rigor paradigm developed in this report will provide the best quantitative description of propellant burning rate (and the gas-phase effects of modifiers on burning rate) for many years to come, possibly to be supplanted by molecular-dynamics descriptions of detailed condensed- and inter-phase processes. The multi-ingredient model has been formalized into a computer code called CYCLOPS after the race of mythical creatures charged with forging thunderbolts for Zeus. It is hoped that it will play a role in developing the next generation of high-performance gun propellants.

2. Single-Ingredient Model

A key objective in the modeling of energetic-material combustion is the development of a mathematical description of the transformation of an ambient-temperature energetic solid in stable chemical disequilibrium into a high-temperature, multicomponent gas at equilibrium. This transformation involves a considerable complexity of physical and chemical processes. The energetic material may decompose in the condensed phase, undergo considerable reaction there, and may form a liquid layer at the burning surface. Gases may be evolved from these subsurface

reactions and either dissolve in the liquid, or form bubbles, or both. At the surface, gases may be produced by reaction or evaporation or both. In general, many reactive species are formed at or near the surface. There they undergo a complex sequence of reactions influenced by the transport of heat and species from one part of the flame to another by convection, diffusion, and thermal conduction. As previously stated, our knowledge of the chemical and physical process in the condensed phase is scant. Furthermore, methods to elucidate these processes with reliability have yet to be developed. Our understanding of and ability to describe the transport processes and reactions in the gas phase, on the other hand, is quite highly developed. In the gas phase, even if a particular reaction's rate and its products are uncertain, the means to measure or calculate these data to greater precision are, for the most part, available. Unfortunately, our ignorance of the condensed-phase processes deprives us even of the types and numbers of chemical species emerging from the surface and their rates of emergence, i.e., critical boundary conditions required for the sophisticated gas-phase calculations. Eventually, reactive molecular-dynamics calculations may supply the necessary condensed-phase descriptions, but, given the primitive state of reactive force fields at present, we believe that time is many years away.

Our interim solution[2] to this dilemma was to estimate the identities and mole fractions of species emerging from the condensed phase and describe their mass rate of emergence by the conventional pyrolysis-law formalism. Since the pyrolysis law must, at present, be measured, such a strategy would effectively be useless if a pyrolysis law must be measured for every ingredient and combination of ingredients. After decades of work, Zenin[3] has shown that double-base (DB) propellants with nitroglycerine (NG) components ranging from 0% to 50% and nitrocellulose (NC) of percent nitration ranging from 11.5% to 13.5% can all be described by a universal pyrolysis law. Furthermore, this same law holds for DB propellants with cyclotetramethylenetetranitramine (HMX) and various catalytic additions. This remarkable finding motivated the hybrid-rigor approach described above. The resulting model was shown to provide good results for the burning rate of frozen ozone, NG, and cyclotrimethylenetrinitramine (RDX).[2] The tantalizing possibility of using the approach as a formulation aid was also demonstrated by the first application of a detailed-chemistry energetic-material model to binary mixtures of NG with a few simple molecular additives.

A mathematical derivation of the basic model and its relation to previous work is given in detail elsewhere[2]; however, a brief summary of the key relationships will be given here to aid the continuity of development. The model treats two computational domains, the condensed phase and the gas phase. In the condensed phase two key assumptions are made: in-depth reactions are negligible and molecular diffusion is negligible. These assumptions enable a derivation of the energy-flux boundary condition at the surface in the following form[2]

$$\lambda_g \left(\frac{dT}{dx} \right)^{+0} = \dot{m} \sum_{i}^{N} \left(Y_i^{-0} h_i^{+0} - Y_i^{-\infty} h_i^{-\infty} \right) \quad . \tag{1}$$

Here N is the total number of chemical species in all phases that is being considered. In this equation λ_g is the thermal conductivity of the gaseous mixture at the surface; $\dot{m}$ is the mass flux eigenvalue; Y_i^{-0} is the mass fraction of the ith species on the condensed-phase side of the surface; h_i^{+0}

is the enthalpy of the ith species on the gas-phase side of the surface; $Y_i^{-\infty}$ is the mass fraction of the ith species in the unreacted propellant; $h_i^{-\infty}$ is the enthalpy of the ith species in the unreacted propellant. Note that the set $\left\{Y_i^{-0}\right\}$ defines the distribution of gas-phase species we assume evolves from the condensed phase, which in this work is assumed to be independent of pressure, while the set $\left\{Y_i^{-\infty}\right\}$ is simply the propellant-ingredient mass fractions. Thus, the term on the right side of equation (1) represents the heat required to change the propellant ingredients (in their initial state) to our assumed condensed-phase product distribution (in the gaseous state) and the quantity on the left side of the same equation is, of course, the heat feedback from the gas-phase reaction zones. Note also that this version of the boundary condition has the very great advantage of requiring only the enthalpy of the starting material at the initial temperature and only the enthalpies of the condensed-phase decomposition products *in the gas state* at the surface temperature. Thus, the highly uncertain thermochemical and thermophysical properties of the expanding and possibly melting condensed phase near the surface are not needed. The price of this reduction in required data is that the model cannot compute the temperature profile through the condensed phase(s), except under the further assumption of constant thermal properties there. This compromise, however, is not a serious limitation to our goals.

In the two-phase steady-state combustion problem there are normally two eigenvalues: the mass flux $\dot{m}$ and the surface temperature T_s. In the present model the number is reduced to only one eigenvalue, conveniently taken as $\dot{m}$, by virtue of the semi-empirical pyrolysis-law relationship

$$\dot{m} = A_s e^{-E_s/RT_s} \quad . \tag{2}$$

The solution proceeds, then, by providing a starting guess for $\dot{m}$ and computing the corresponding surface temperature from equation (2). This defines the equivalent of a burner-stabilized flame problem with elementary reactions. We modified the PREMIX code[4] to solve the gas-phase conservation equations, and CYCLOPS calls this modified code as a subroutine. The gas-phase solution then determines the heat feedback to the surface [left side of equation (1)]. The results are checked to see if the surface energy-flux boundary condition, equation (1), is satisfied. If not, a new value of $\dot{m}$ is chosen by an algorithm and the whole procedure iterated until the eigenvalue is found. These iterations are continued until the difference in mass fluxes associated with successive iterations is less than 1%. Furthermore, since the length of the computational domain (the keyword XEND in PREMIX) can affect the heat feedback, the CYCLOPS code automatically extends this domain until successive computations of the heat feedback differ by no more than 1%. Experience indicates that these criteria provide burning rates that are accurate to within a few percent.

It is worth pointing out that the success of the single-ingredient model depends *largely* on getting three inputs right: the pyrolysis law, the net condensed-phase decomposition products, and the gas-phase reaction mechanism. (Other data, such as the heats of formation of the ingredients, may also play a significant role [see below].) The pyrolysis law may, in principle, be obtained either

by theoretical or experimental means. An example of the theoretical path was given previously[2] for the case of frozen-ozone deflagration. In that case, a law in the form of equation (2) was fit to detailed calculations of an evaporation surface-regression mechanism. For more complex energetic materials, measurements of the pyrolysis law are generally required. As for the (nonequilibrium) decomposition products of the condensed-phase, so long as there is a sharply defined surface boundary, one can say that there will exist some such set of decomposition products at the surface of every deflagrating energetic material. We may not be able to discern easily what this set is, but at least the concept that such a set exists is sound. The implicit assumption that the products of the condensed-phase decomposition do not change with pressure is harder to justify. Without pressing the point too vigorously, it is nonetheless worth observing that the burning rate of most propellants varies over many decades of pressure as a power law in pressure. This same dependence arises from overall-reaction models, which also have reactants unchanging with pressure.[5] Such an argument is admittedly inferential, but it is suggestive that the assumption of pressure-independent surface products may not be inappropriate to the propellant problem. In any case, the mathematics of the model developed here do not depend on the assumption that the condensed-phase product set is independent of pressure; if known, changes in the product set with pressure could easily be included. Finally, though a given gas-phase reaction mechanism may be imperfect, there exist theoretical and experimental techniques to improve the description of practically any elementary reaction, given sufficient resources. Thus, a successful calculation of burning rate using this model must be possible even if the detailed condensed-phase processes are not known, provided that accurate information for the inputs previously mentioned can be found. The model should therefore be a durable and versatile framework for quantitatively incorporating new research results on the detailed processes of propellant combustion.

The semi-empirical approach taken here, requiring as it does estimates of the chemical products of the condensed-phase reactions, may appear to be less rigorous and more speculative than models that hypothesize specific reaction paths in the condensed phase and compute their effects explicitly. On the contrary, we believe that those models which treat the condensed-phase processes explicitly are far more speculative than what we have proposed, given the current impoverished state of knowledge of those processes. In those models, not only must surface gasification mechanisms and specific reaction paths be hypothesized, but also the reaction rate parameters must be estimated. This argument was posited in greater detail previously.[2]

3. Multi-Ingredient Model

A practical solid propellant is almost always a mixture of ingredients. This fact poses a number of new problems beyond those inherent in the single-ingredient model. One such problem is the issue of determining the total starting-material enthalpy. Enthalpies of solution and mixing logically should be included, so that the enthalpy of the propellant is not simply the sum of the

enthalpies of the ingredients as assumed in the derivation of equation (1). In practice, however, such refinements are not normally considered in thermochemical-equilibrium calculations for propellants. This neglect is, for the most part, due to the unavailability of these interaction energies though some justification may be found in the fact that such energies are generally relatively small corrections to the sum of the ingredient enthalpies. Molecular dynamics calculations may some day be routine in computing the total enthalpy of the propellant amalgam; however, for the present, we follow the expedient convention of summing the ingredient enthalpies. It should be noted, however, that these effects may not always be insignificant. In computing the enhancement of the linear burning rate of NG by adding a small amount (2.4% by weight) of NH_3, we previously found[2] that using the gaseous-state enthalpy for NH_3 results in a 19% burning-rate boost, whereas using the liquid-state enthalpy of NH_3 produced only a 12% boost. The reason is that more of the gas-phase heat feedback is "wasted" in supplying the latent heat of vaporization in the latter case. Enthalpies of solution or mixing are presumably closer in magnitude to enthalpies of fusion than to enthalpies of vaporization, so that the effect should be generally smaller than suggested by this example; one should nevertheless bear in mind that the propellant enthalpy is presently only approximated and that the effect of this approximation on the burning rate is not readily assessed.

Another issue that arises in the multi-ingredient model involves the net gaseous decomposition products evolving from the condensed phase of the propellant mixture. There is the distinct possibility that, during reactive condensed-phase decomposition, the products evolving from the mixture may not be the same as those from the non-interacting component ingredients. This may happen either because the presence of one ingredient may alter the course of decomposition of another ingredient or because of reactions between the ingredient products in the condensed phase. In this work, however, we assume that no such interactions occur, i.e., that the propellant decomposition-product mole fractions may be computed from the decomposition products of each ingredient according to the proportion of each ingredient in the propellant. As with the mixture enthalpy problem just discussed, there is little recourse to this approach at the present time. Unlike the mixture enthalpy problem, however, we have little evidence for believing this procedure to be a good approximation. On the other hand, in the absence of further understanding about the condensed-phase reactions, this approach is certainly reasonable and least biased in an *a priori* sense. Its justification must come largely from whatever success the model enjoys by its employment. It may well turn out that the assumption of non-interactive decomposition works well for some combinations of ingredients but not for others.

The net mole fractions of condensed-phase products arising from the propellant mixture is therefore calculated as follows: Suppose that the unreacted-propellant ingredient mass fractions are given by $Y_i^{-\infty}$ ($i = 1, \mathrm{I}$) and that one mole of ingredient i produces n_{ij}^{-0} moles of condensed-phase product species j. If W_j is the molecular weight of species j and X_j^{-0} is the mole fraction of product species j on the condensed-phase side of the surface, then the net mole fraction X_k^{-0} of product species k on the condensed-phase side of the surface due to all ingredients is given by

$$X_k^{-0} = \frac{\sum_i^I \left(\frac{Y_i^{-\infty}}{W_i} n_{ik}^{-0} \right)}{\sum_j^J \sum_i^I \left(\frac{Y_i^{-\infty}}{W_i} n_{ij}^{-0} \right)} \tag{3}$$

where J is the total number of different product species from all of the ingredients. The set of mole fractions $\left\{ X_k^{-0} \right\}$ are the boundary conditions required for solution of the gas-phase species-conservation equations. In sum, we find a set of decomposition products that leads to a reasonably good computed burning rate for each ingredient, then compute by the above equation the net mole fractions of each surface product produced by all the ingredients, properly weighted by the relative amounts of the ingredients that make up the propellant.

Mass density of the propellant mixture is computed by the simple method of additive partial molar volumes as described in reference 2 and given by the equation

$$\rho_{mix} = \frac{W_{avg}}{\sum_i X_i V_i} \tag{4}$$

where W_{avg} is the average molecular weight of the propellant mixture, X_i is the mole fraction of ingredient i, and V_i is the molar volume of ingredient i. This approximation assumes negligible distortion of the pure-ingredient molar volumes by the dissimilar-molecule interactions. It is the best approach one can take short of molecular-dynamic simulations for each case. (See the end of the next section for more discussion.)

The accuracy of the multi-ingredient model will naturally depend (at best) on the accuracy with which the model reproduces the burning rates of the pure ingredients. Rather than this fact being a disadvantage, we expect that the predicted burning rate of the multi-ingredient model will be somewhat forgiving of inaccuracies in any single ingredient simply because the overall degree of integration is higher. It is well known among combustion modelers that often the burning rate is surprisingly insensitive to the details of the underlying processes; it is hoped that this experience will work to our advantage in the multi-ingredient model.

4. Nitrocellulose, A Special-Case Ingredient

Nitrocellulose (NC) is a major ingredient in conventional smokeless propellants. It is also an ingredient presenting formidable complexity to the modeler. NC exists as a long-chain polymer with three potential nitration sites on each monomer. The monomer with all sites nitrated, cellulose trinitrate, is depicted in Figure 1. The three carbon-atom nitration sites are labeled in the figure as *2*,*3*, and *6*. If at one or two of these sites the O-NO2 group is replaced by an hydroxyl group, the resulting monomers are referred to as cellulose dinitrate and cellulose mononitrate, respectively. A given specimen of NC is characterized by an average nitration level expressed as the percent of nitrogen-atom mass to average monomer mass. The average percent nitration *%N* is related to the average number of nitrate groups per monomer, $\overline{n}_{NO_2}$, by the definition

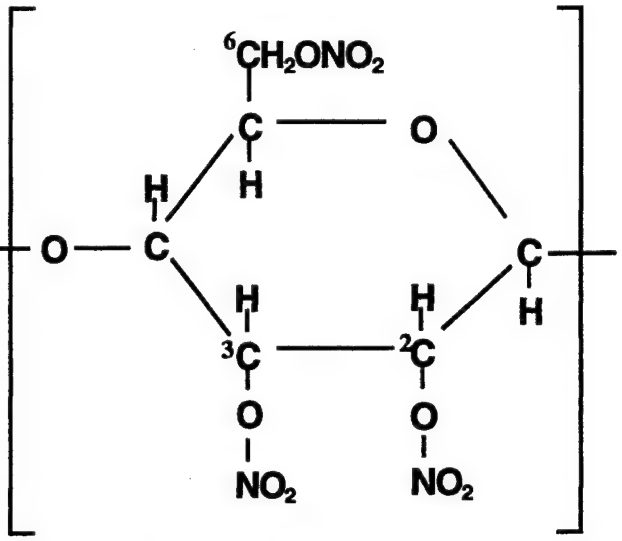

Figure 1. Schematic representation of cellulose trinitrate monomer.

$$\frac{\%N}{100} \equiv \frac{\overline{n}_{NO_2} W_N}{\overline{W}_{NC}} \quad . \tag{5}$$

where W_N is the molecular weight of the nitrogen atom and $\overline{W}_{NC}$ is the average monomer molecular weight in the NC specimen. From this relation one can determine that the percent nitration corresponding to the pure mononitrate is 6.76%, to the pure dinitrate is 11.11%, and to the pure trinitrate is 14.14%.

Since military nitrocellulose is typically in the range of 12 %N to 13 %N, one might at first suppose that it consists of a mixture of only di- and tri-nitrates, but this is not the case. Leider and Seaton[6] have investigated the distribution of nitration states, i.e., the fractions of mononitrates, dinitrates, and trinitrates, for an NC specimen of given average percent nitration. They performed Monte-Carlo calculations for two cases depending on different assumptions as to the probability of nitration at given sites. In one case, nitration at sites 2, 3, and 6 were considered equally probable, which results in some monomers being unnitrated, and in the other they assumed at least one site was always nitrated. Their assumed nitration level was 12.15 %N, which was chosen to match their test specimens. They also examined the case of at least two sites being nitrated; this case can be done

analytically. The case which best fit their thermal-decomposition experiments, involving weight loss and gas evolution, was the one where at least one site was always nitrated.

Using the findings of Leider and Seaton[6], we developed our own Monte-Carlo code to determine the distribution of nitrate states for a given value of average percent nitration. We assume that, for military NC, at least one site is nitrated and that C6 is the preferred site. This choice is consistent with the isotope-substitution work of Gelernter et al.[7], who established that the nitrate group at the C6 position is the most stable. The remaining sites, C2 and C3, are considered equally probable for nitration. The assumption that C6 is the most stable while C2 and C3 are equally probable is also supported by quantum-mechanical structure calculations.[8] The Monte-Carlo code, a subroutine of CYCLOPS, works as follows. First, the given percent nitration is converted to the average number of NO_2 groups per monomer, $\overline{n}_{NO_2}$.

$$\overline{n}_{NO2} = \frac{\left[\frac{\%N}{100}(6W_C + 10W_H + 5W_O)\right]}{\left[W_N - \frac{\%N}{100}(W_N + 2W_O - W_H)\right]} \qquad (6)$$

This relation follows after a little algebra from equation (5). One then considers an NC system consisting of n_{mon} monomers. Since for mititary nitrocellulose we assume that the C6 position is always occupied by an NO_2 group, $n_{mon}(\overline{n}_{NO_2} - 1)$ is the number of excess NO_2 groups to be distributed among the ($2\ n_{mon}$) available C2 and C3 sites in the NC system. In the Monte-Carlo description, no distinction is made between dinitrates with C2 occupied by an NO_2 group and those with C3 occupied (although we have hypothesized that the decomposition product sets are different). This distribution is done randomly and the result defines one system configuration. The process is repeated for many configurations and the distribution fractions compiled as averages over all the configurations. Experimentation showed that a system consisting of 1000 monomers and 1000 configurations was sufficient to maintain two-place precision in the distribution fractions and such precision was considered commensurate with that of other data used in the burning-rate calculation. Figure 2 illustrates how the distribution among nitrate states varies with the given percent nitration according to this model.

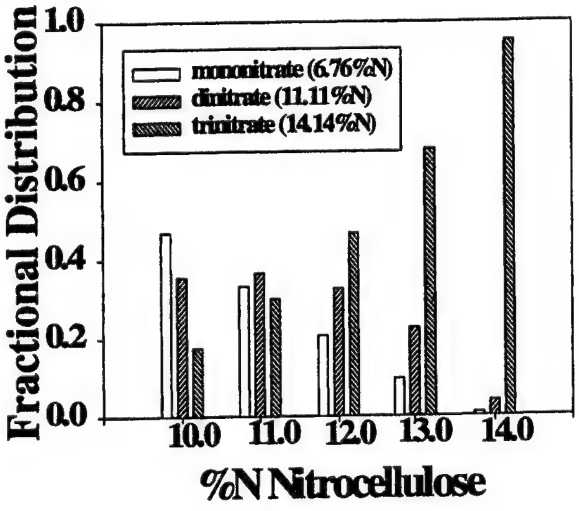

Figure 2. Nitrate-state distribution according to the Monte-Carlo code.

Recent experimental work allows a more direct test of the Monte-Carlo model predictions than did the experiments performed by Leider and Seaton.[6] Todd and Glasser[9] used NMR spectroscopy to determine the distribution of

nitrate groups in the NC repeat units, or what we have more loosely termed the NC monomers. Their data for NC specimens of two different nitration levels and several blend samples of the same percent nitration are shown along with our Monte-Carlo model predictions in Figure 3. It can be seen that the model simulates the distribution with uncertainties that are of the order of the measured variations, which are due both to experimental errors and to variances in the homogeneity of the NC samples themselves.

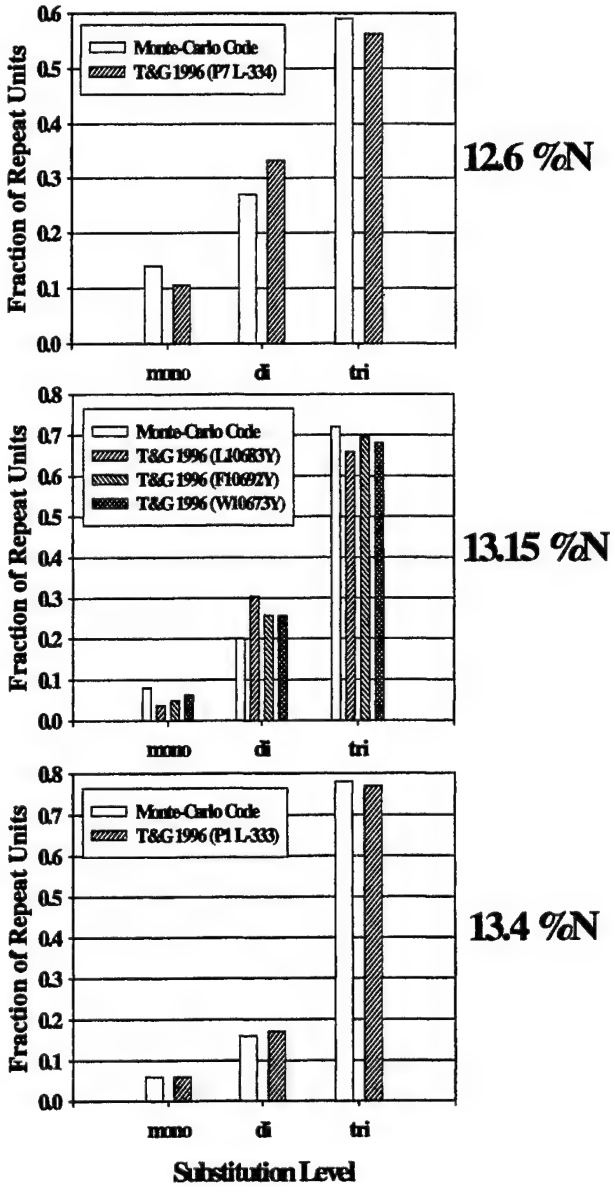

Figure 3. Comparison of Monte-Carlo code predictions of nitrate-state distributions to NMR measurements of Todd and Glasser.[9]

With the Monte-Carlo model in hand, NC as a propellant ingredient is treated in the burning-rate model as comprising three separate ingredients: cellulose mono-, di-, and tri-nitrate. One must provide properties and a set of decomposition products for each of these substituents in the ingredient database (discussed in the next section). The heats of formation (on a per-mole basis) of the different states of nitration of NC are obtained from a second-degree-polynomial fit (shown in Figure 4) to data derived from the per-gram heat-of-formation expression reported by Taylor, Hall, and Thomas.[10] The mass densities of each of the nitration states are required as well, and these were obtained by molecular-dynamic simulations of the homopolymers using the COMPASS force field.[8] The results are as follows:

cellulose mononitrate

$\rho = 1.5250$ g/cm^3,

cellulose dinitrate

$\rho = 1.5778$ g/cm^3, and

cellulose trinitrate

$\rho = 1.6640$ g/cm^3.

Using these homopolymer densities, the measured densities of other ingredients, and the code-assumed propellant formulations given in Table 1, we compare the values predicted by equation (4) to measured propellant densities[11] in Table 2. The densities are predicted to within about 1% in all cases except M10. A single-base propellant, M10 is poorly plasticized and may well include voids created during the drying process; this would cause a prediction error in the direction seen. Accurate

prediction of the density for such propellants may require a molecular-dynamic simulation which accounts for the migration of solvent from the molecular interstices during drying.

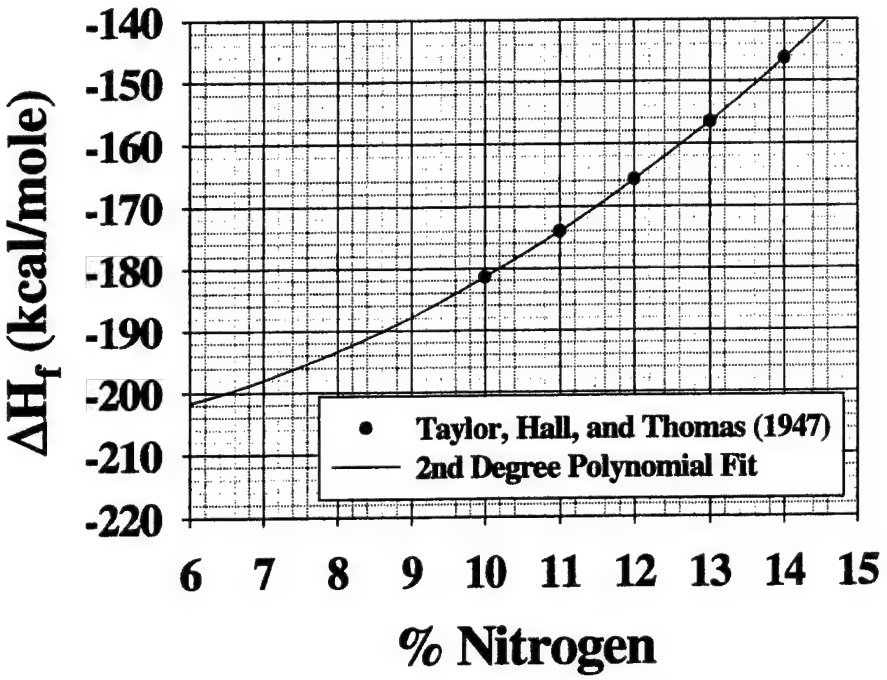

Figure 4. Heats of formation of nitrocellulose as a function of percent nitration generated as an analytic fit to the measurements of Taylor et al.[10]

5. The Ingredient Database: A Work in Progress

Though vastly more complex, the CYCLOPS code works much like a thermochemical equilibrium code in that it reads an input file containing the name of the propellant, the names and weight fractions of each of the ingredients, the initial temperature, and the pressure for which the burning rate is desired. If a propellant includes NC as one of its ingredients, an input value of the percent nitration is also required; in that event, a call is then made to the Monte-Carlo subroutine, which returns the molar fractions of mono-, di-, and trinitrates. The properties of each ingredient, including molecular weight, mass density, specific heat, heat of formation, and condensed-phase decomposition products, reside in an ingredient database file, which is read as required by the CYCLOPS code.

At the present time, there is no way to remove an element of speculation in setting down the condensed-phase decomposition products evolving from the surface from each ingredient, so it is to be expected that the ingredient database will be a work in progress, being refined as experience, new experiments, or theory suggest better choices. The only conservation principle constraining the

choice of these decomposition products is elemental balance in writing the overall chemical reaction from unreacted compound to products. Beyond that, for guidance one might appeal to thermal-decomposition experiments, though awareness of the possible role of heating rate and secondary reactions may limit the suitability of many of these experiments. Also, one might argue by analogy with reaction paths for known reactants or reactant subgroups or, even more crudely, base arguments on average bond energies. Finally, one is constrained by the practical requirement that the reaction mechanism must include any proposed decomposition species, though the mechanism certainly may be expanded, with varying degrees of difficulty, to include new species as required. Of course, an obvious criterion is the degree to which use of a particular set of ingredient products leads to a calculated burning rate which agrees with experiment. Use of this last criterion presupposes a high level of confidence in the pyrolysis law and gas-phase reaction mechanism. Variation of the burning rate with different condensed-phase decomposition-product sets was illustrated previously for NG.[2]

Ideally, the best set of decomposition products to use for a given ingredient would be determined by computing the burning rate for the neat ingredient based on many possible sets and accepting the one that is both theoretically sound and leads to the best agreement with experimental burning rates. Several circumstances can interfere with this approach. Experimental burning-rate data may not be available for some ingredients or, as in the case of each nitration state of NC being considered a separate ingredient, it may not even be possible to prepare a pure form of the ingredient for experimental test. Some secondary energetic ingredients burn much more slowly than the main energetic ingredients and prove to be troublesome with regard to achieving convergence in the PREMIX code. Finally, some ingredients, such as inert binders, will not undergo self-sustained combustion at all. In all these cases, one simply has to do the best one can and be open to improvements. For example, cellulose trinitrate has a %N of 14.14%, but the most similar material for which we have burning rates is M10 propellant with a %N of 13.15%. (see Table 1.) Therefore, we expect that cellulose trinitrate will have a burning rate somewhat higher than M10. We investigated about two dozen different condensed-phase decomposition sets for cellulose trinitate, most of which led to burning rates much above or much below the experimental burning rate of M10, which is a mixture of nitration states. We selected the set that produced burning rates somewhat above that of M10, allowing for the energy-diluting effects of the lower nitrate states in the propellant compared to a pure cellulose nitrate. Our universe of tested decomposition sets was not (probably could not have been) comprehensive; there may well exist a better choice. The one selected, however, does result in reasonable agreement for the range of propellants examined. The decomposition sets for the dinitrate and the mononitrate were then selected by analogy with the decomposition scheme of the trinitrate. It should be stressed that, once a set of decomposition products is established for a particular ingredient, that set is fixed for all propellant formulations using the ingredient. This is the source of our claim for predictability.

The ingredient database used for the calculations reported here is given in Appendix A. The net mole fractions of the decomposition products from each of the propellants, resulting from the decomposition of each of their respective ingredients, are collected in Table 3. Values for heats of formation for all of the ingredients except for NC were taken from the Hunter thermochemical

equilibrium code.[12,13] Where more than one value for an ingredient is given in the Hunter database, we used the average value.

Table 1. Weight-percents of propellant ingredients according to nominal specifications: actual/code-assumed.

Ingredient	Propellant			
	M10	M2	M9	JA2
NC	98.0/100	77.45/79.9	57.75/59.1	59.50/60.0
%N	13.15	13.25	13.25	13.1
NG	-	19.50/20.1	40.0/40.9	14.90/15.0
DNT	-	-	-	-
DEGDN	-	-	-	24.80/25.0
NQ	-	-	-	-
DBP	-	-	-	-
DPA	1.0/0	-	-	-
EC	-	0.60/0	0.75/0	-
DEP	-	-	-	-
$BaNO_3$	-	-	-	-
KNO_3	-	2.15/0	1.50/0	-
KSO_4	1.0/0	-	-	-
Graphite	-	0.30/0	-	0.05/0
AlF_6Na_3	-	-	-	-
MgO	-	-	-	0.05/0
Akardit II	-	-	-	0.70/0

Table 2. Comparison of measured[11] propellant densities (in g/cm^3) and present predictions using equation (4).

Propellant	Predicted Density	Measured Density	% Error
M10	1.638	1.51 ± 0.01	8.5
M2	1.630	-	-
M9	1.620	1.62 ± 0.02	0
JA2	1.558	1.57 ± 0.01	- 0.8

Table 3. Summary of computed net mole fractions of condensed-phase decomposition products.

Decomposition Product	Propellant			
	M10	M2	M9	JA2
NO_2	0.2930	0.3204	0.3466	0.2771
HONO	-	0.0115	0.0243	0.0579
CHOCHO	-	-	-	0.0211
HCO	0.1111	0.1092	0.1071	0.1050
CH_2O	0.2222	0.2414	0.2627	0.2415
CH_2	0.1111	0.0919	0.0706	0.0919
CH_3	-	-	-	0.0140
CH_4	-	-	-	0.0070
CO	0.2222	0.1954	0.1655	0.1574

6. The Gas-Phase Reaction Mechanism: A Work in Progress

The gas-phase reaction mechanism is much more solidly based in experiments and theory than are the suppositions as to the condensed-phase decomposition products; yet, like the ingredient database, it also must be considered a work in progress. New information on heats of formation, specific heats, reaction rates, and products of elementary reactions are continually becoming available, requiring periodic updates in the reaction mechanism. As our present reaction mechanism comprises 59 chemical species and 365 reversible reactions, it can readily be appreciated that updating both the reaction mechanism and all of the consequent burning-rate calculations is not a trivial exercise. The reaction mechanism utilized for the present calculations is provided in Appendix B. It is to be expected that updates to the reaction mechanism may well result in poorer agreement between the predicted burning rates and experimental ones. One might then have to modify the decomposition products to recover acceptable agreement between predicted and theoretical burning rates.

The present mechanism is much larger than the one used for our single ingredient calculations.[2] Like the previously used mechanism, the present one started from a version of our dark zone mechanism.[14,15,16,17] In the previous work,[2] we attempted to pare down the number of reactions, primarily by intuitive guesses that certain species might not matter rather than actual comparative calculations. The reason for this approach was that the computational resources available were being strained to their limits. Since that time, computational resources have improved. We now find that some of the reactions left out are, in fact, important. In particular, we had deleted 10 species (HCN, HNCO, HOCN, HCNO, CN, H_2CN, C_2N_2, HNC, NCNO, NCN) and about 70 reactions which describe the HCN/HNCO chemistry. (Note that NCO was included in the previous mechanism.) At the time we thought that these deleted species and reactions were only likely to matter for nitramine ingredients, but it turns out they are formed in trace amounts and are important in the dark zones of nitrate esters (see subsequent discussion in Section IX). Another major change from the dark-zone mechanism is the addition of many reactions pertinent to CH_4/O_2 combustion taken from the Gas Research Institute consortium mechanism 2.11.[18] These are denoted by the symbols <=> replacing = in Appendix B.

Additionally, we now find that two HCO + HCO reactions producing different product sets (R355 and R356, where R355 means Reaction 355 in Appendix B) are very important. Since our previous[2] product set for the single ingredient NG included HCO, leading to a high concentration of this species in the near surface region, we suspected inclusion of these reactions might lead to a big change in predicted NG burning rates. Indeed, it does cause predicted rates to increase strongly, due to increased near surface heat release, necessitating a change in assumed surface products for that ingredient (see Appendix A).

Another major difference is that chemistry of ketene (CH_2CO) and glyoxal (CHOCHO) has been included. It was thought these species might actually play a role as surface products, so they were tried as such for several of the trial ingredients. Although only the latter species is retained as an assumed surface product (for DEGDN), ketene formation near the surface is very important as $CH_2 + CO + M = CH_2CO + M$ (R358, which means the reverse of R358) is very important for near surface heat release and, consequently, for the heat feedback.

Finally, the last major change is that the rate coefficient of R19, $HNO + NO = N_2O + OH$, as been increased by a factor of two. It has long been known that calculations of dark zone structure are highly sensitive to this reaction, especially for nitrate ester propellants.[14,15,16,17] The rate coefficient previously used was obtained from the excellent review by Diau et al.[19], in which they carefully analyzed their group's own new experimental data, and all prior data (see quoted references in reference 19), from static reactor experiments on H_2/NO mixtures. Unfortunately, in the analysis, they used an ancillary datum for the heat of formation of HNO which is now known to be in error.[20] In unpublished work, Anderson has shown that calculations for the H_2 /NO mixtures and for propellant dark zone length are very sensitive to this heat of formation. The reason is that R3 and R161, which strongly influence the [HNO], have non-negligible rates in both directions†; thus, since the rate coefficients of back reactions are computed from the thermodynamics, the heat of formation of all the species involved affects the computed [HNO]. The change in heat of formation causes the computed [HNO] to decrease by about a factor of two; thus, to keep the rate of R19 the same vs. the H_2/NO kinetics data, k19 (the rate coefficient of R19) must be increased a factor of two.# We

---

† One can gain an understanding of the situation by assuming that R3 and R161 are in partial equilibrium, whence an expression for the amount of change induced in computed [HNO] induced by the revised heat of formation can be derived analytically. This assumption is only roughly correct over the range of conditions of interest. However, the concentration change predicted in this way is about a factor of two. We have not attempted to determine whether an assumption of partial equilibrium for these reactions could be successfully used as part of a reduced dark zone model.

This factor was found to apply uniformly over the entire range of experiments performed or quoted in reference 19. It should be noted that M.C. Lin, in a private communication, has cautioned that an increase by a factor of two in the rate coefficient of R19 makes agreement with the transition state theory calculations of the rate coefficient (see reference 19, and references therein) somewhat tenuous at the high temperature end of the range studied (900 - 1430 K). Typically, one currently expects the best work to result in agreement within a factor of about 3, but our proposed 2x increase leads to agreeement only within a factor of 5. Lin pointed out this suggests there might be some moderately important radical source reaction missing from the mechanism. We agree that this might be the case, but it might also be that our increased rate coefficient is correct and the agreement is simply a little worse than usually obtained in such comparisons; or perhaps the calculated constant needs to be revisited. Until such a reaction or reactions are found, we suggest using our updated k19 in conjunction with the revised HNO heat of formation.

recommend using the revised HNO heat of formation because this may influence other reactions as well; this forces use of the increased k19. R19 is an important radical source for propellant dark zones, especially for nitrate esters. We find that using the Diau et al.[19] value for k19 increases the predicted nitrate ester dark zone lengths by about a factor of two from those given in our figures (see Section VIII), and do not agree well with experiment.

7. Burning-Rate Predictions

The primary objective of CYCLOPS is to predict the burning rate of a propellant as a function of its ingredients. Emphasis here is on the word "predict." While our choice of condensed-phase decomposition-product set for a given ingredient may be influenced by the best agreement with the experimental burning rates for that pure ingredient, once determined, the decomposition products for each ingredient are considered fixed for purposes of computing burning rates for all the propellants which include that ingredient. Under these constraints and in the face of the considerable uncertainties associated with the legion input parameters, agreement between the predicted and experimental burning rates should be judged successful if they are within a factor of two.

To illustrate the application of the model to nitrate-ester propellants, calculations were performed on a set of four standard U.S. Army gun propellants including single-base, double-base, and triple-base propellants. We have thus far not attempted to include minor ingredients such as stabilizers; thus the nominal formulations are renormalized to reflect these small omissions. The nominal and code-assumed formulations are given in Table 1.

The results for the single-base propellant M10 are shown in Figure 5. M10, with an average number of NO_2 groups of 2.64, is chosen as our prototype for cellulose trinitrate; it has the highest nitration level (13.1%N) of any nearly pure nitrocellulose (98% NC) for which we had burning-rate data. Two of the three sets of

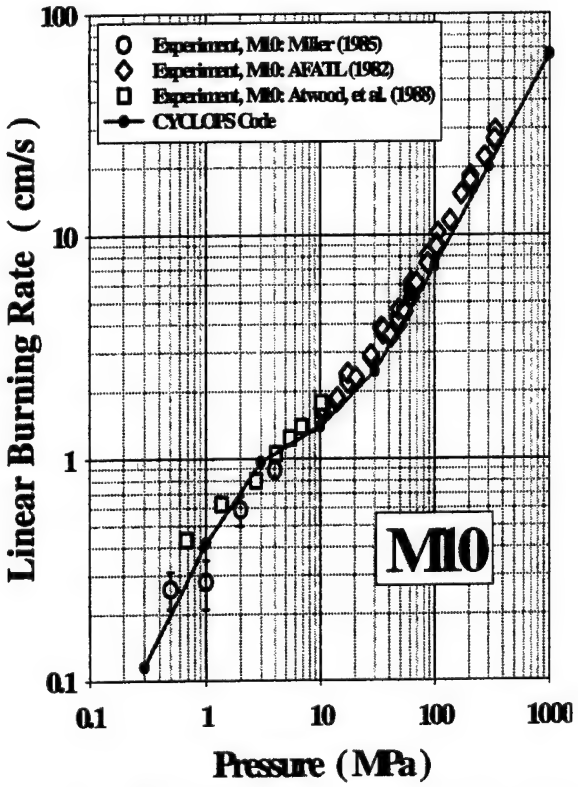

Figure 5. CYCLOPS-computed burning-rate pressure dependence for M10 compared to experiments[22,21,23] at an initial temperature of 294 K.

burning-rate measurements[21,22] were performed with the same single-batch lot of M10 propellant; the third set of measurements[23] is very consistent with the first two. The CYCLOPS code results are in excellent agreement with these data, even to include the gentle inflection evident at about 10 MPa.

In order to address double-base propellants (and JA2), one needs to have nitroglycerine (NG) and diethyleneglycol dinitrate (DEGDN) in the ingredient database. In previous work,[2] we found a set of decomposition products for NG that worked well to reproduce the burning rates for the gas-phase reaction mechanism then in use. Since that time, we have improved and updated the reaction mechanism and found that the former "best" decomposition products failed to give satisfactory burning rates with the new mechanism. This illustrates some of our cautionary remarks in the ingredient-database discussion above. A new "best set" was found and is used in this work. Of course, there is no guarantee that further improvements to the reaction mechanism, itself a work in progress, will not necessitate new sets of ingredient decomposition products. However, the process should ultimately converge to a single "best set" limit. These new products for NG are given in Appendix A, and the computed burning rates for NG based on them are shown in Figure 6 compared to the experimental work of Andreev[24,25] and Andreev et al.[26] The computed rates are in very good agreement with the measurements over four decades of pressure. The burning rates using the best decomposition products we could find for DEGDN are shown in Figure 7 along with experimental data.[27] Improvements may well be possible for this ingredient; however, results for JA2 (below) suggest that the present level of accuracy in the DEGDN product set is probably adequate.

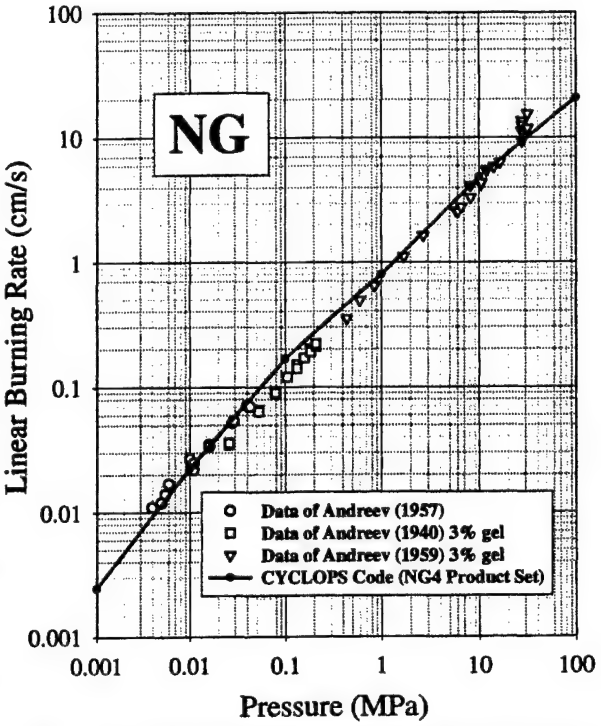

Figure 6. CYCLOPS-computed burning-rate pressure dependence for nitroglycerine (NG) using the NG4 product set compared with experiments.[24,25,26]

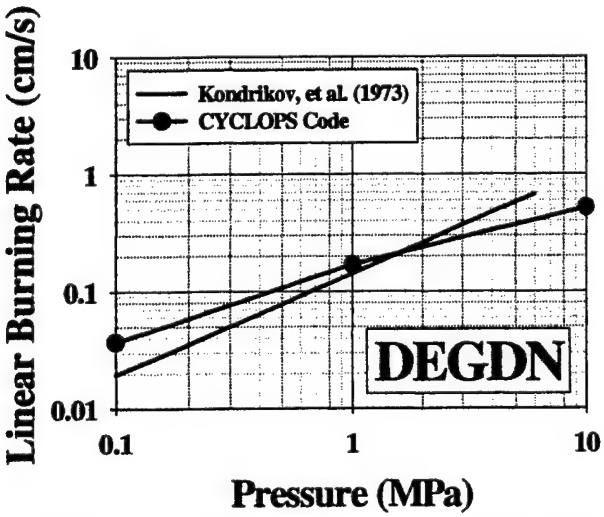

Figure 7. CYCLOPS-computed burning-rate pressure dependence for diethyleneglycol dinitrate (DEGDN) compared to experimental data of Kondrikov et al.[27]

Double-base propellants of widely varying compositions are shown in succeeding figures. M2 propellant (Figure 8) has a relatively low nitroglycerine content, M9 (Figure 9) has a relatively high nitroglycerine content, and JA2 (Figure 10) is similar to M9 but with a substantial amount of the NG replaced by diethyleneglycol dinitrate (DEGDN). Predictions are within a factor of two of the M2 data of Grollman and Nelson[28], the M9 data of Vanderhoff et al.[29] and the Radford Army Ammunition Plant's propellant description document[30], and the JA2 data of Miller[22] and that of Juhasz et al.[31]

One aspect of the burning-rate calculations that proved to be a surprise is the sensitivity of the burning rate to small changes in the heats of formation of the ingredients. This sensitivity is a function of pressure, being small at high pressures and sometimes quite large at low pressures. An example of this sensitivity is shown in Figure 9 where the effects on the computed burning rates of increasing (and decreasing) the heats of formation of all the ingredients by 3% are illustrated. This computational ability might be used to determine the acceptable tolerances of ingredient purity with respect to the burning rate. For example, one could quantitatively determine how much glycerol dinitrate (with its lower heat of formation) could be tolerated in the NG feedstocks.

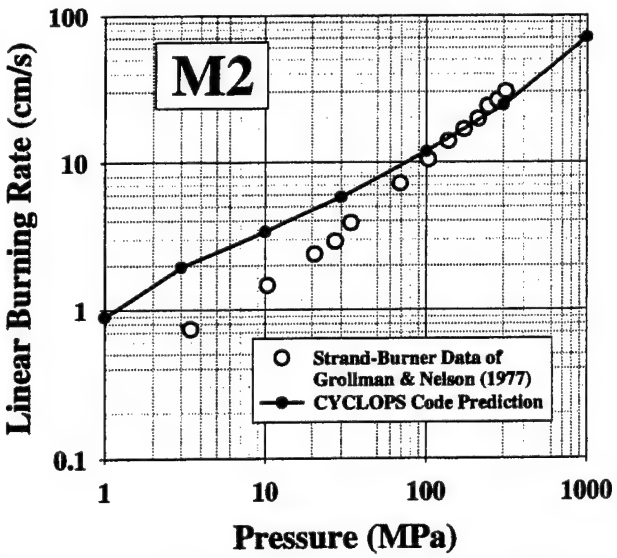

Figure 8. CYCLOPS code prediction of M2 burning-rate pressure dependence compared to experiment[28] at an initial temperature of 294 K.

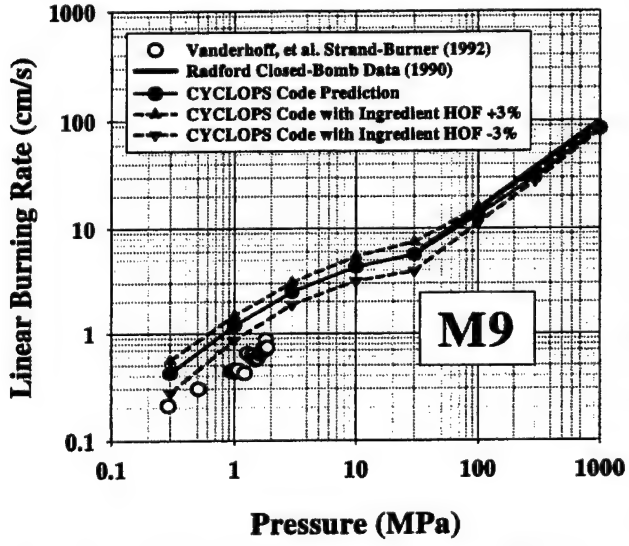

Figure 9. CYCLOPS code prediction of M9 burning-rate pressure dependence compared to experiments[29,30] at an initial temperature of 294 K. Also shown are the effects on the computed burning rates of either increasing or decreasing the heats of formation by 3% for all of the propellant ingredients at once.

A final illustration of burning-rate computations with the CYCLOPS code involves the sensitivity of the burning rate to the initial temperature of the propellant. It is worth asking whether Zenin's pyrolysis law retains its universal character for burning rates at different initial temperatures as well as pressures. Figure 11 shows the pyrolysis law data for many different double-base formulatons along with a few data[32] at 1 atm and 20 atm over a wide range of initial

temperatures. The fitted line does not include these initial temperature data, however, it is clear that the wide-initial-temperature data is reasonably consistent with the ambient-temperature data, justifying our use of the ambient-temperature pyrolysis law at non-ambient temperatures. Eisenreich et al.[33] published measurements of the temperature sensitivity of JA2 burning rates at a number of pressures from 75 MPa to 175 MPa. A comparison of our calculations with their data at the two pressure extremes are shown in Figure 12. The slopes of the predicted and experimental curves, i.e., the change of burning rate for a given change in initial temperature, are fairly close. On the other hand, a commonly used measure is the temperature sensitivity, σ_p, at constant pressure, defined as

$$\sigma_p \equiv \frac{1}{r}\left(\frac{\partial r}{\partial T_0}\right)_p \quad . \qquad (7)$$

Here r is the linear burning rate and T_0 is the initial propellant temperature. If one were to compare σ_p, the agreement would not be as good since

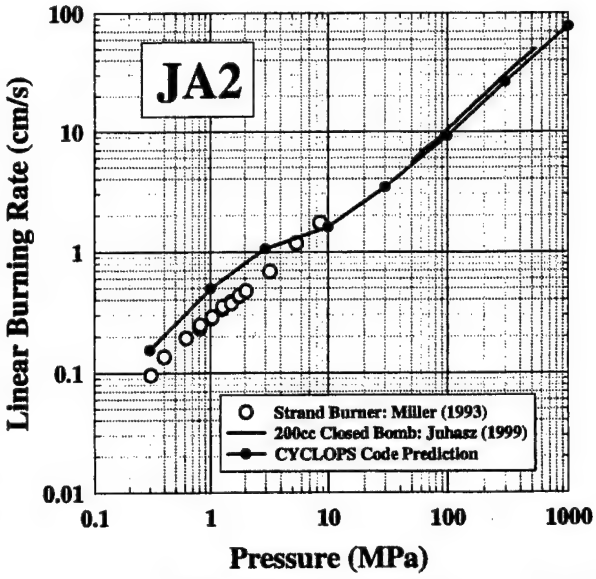

Figure 10. CYCLOPS code prediction of JA2 burning-rate pressure dependence compared to experiment[22,31] at an initial temperature of 294 K.

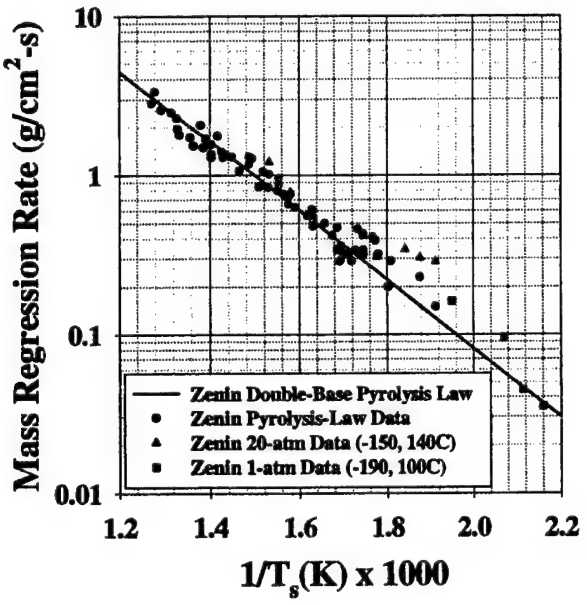

Figure 11. Applicability of Zenin's pyrolysis law[3] to double-base propellants for extreme initial propellant temperatures.[3,32]

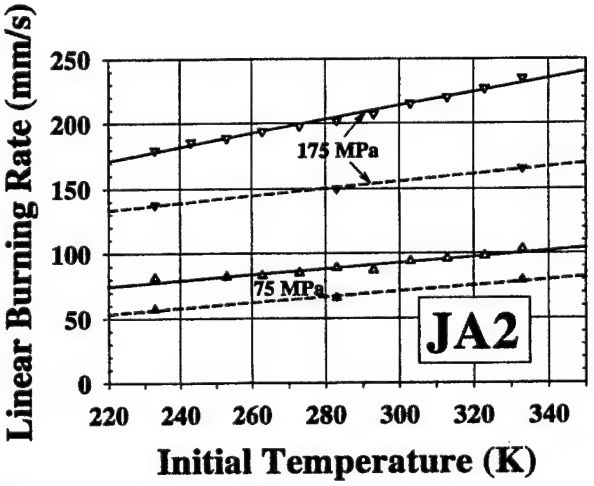

Figure 12. Computed initial-temperature dependence of the burning rate of JA2 at 75 MPa and 175 MPa (solid symbols, dashed linear least-squares fit) compared to the data of Eisenreich et al.[33] (open symbols, solid linear least-squares fit).

this quantity is biased by inaccuracies in the magnitude of the burning rate itself. It is worth noting here that the Eisenreich data is obtained with the German JA2 formulation and this differs somewhat from the U. S. formulation. Both countries use a blend of two NC lots which average to the same percent nitration; however, the two different blended lots have different nitration levels. At present the CYCLOPS model allows for only one lot of NC in a given formulation, but we intend to extend the capability to study this case. Even keeping the average nitration level the same, blending lots of different nitration levels will, by our Monte-Carlo submodel, result in different mole fractions of mono-, di-, and tri-nitrates, and these differences will lead to different burning rates. Indeed, the German JA2 rates are some 20% faster than those for the U.S. material. This illustrates in yet another respect the potential value to formulators of having a quantitative prediction tool such as CYCLOPS.

8. Flame-Structure Predictions

Almost a decade ago Vanderhoff et al.[29] published measurements of gas-phase spatial profiles of temperatures and absolute NO mole fractions for several U.S. Army propellants, including M9 and JA2. These temperature profiles are compared to the predictions of the CYCLOPS code for JA2 at 1.6 MPa in Figure 13 and for M9 at 1.7 MPa in Figure 14. It can be seen that both the magnitude of the dark-zone temperature and the position of

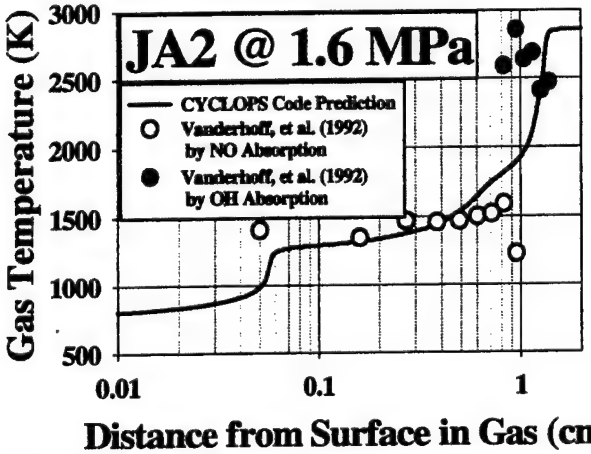

Figure 13. Thermal flame-structure predictions of CYCLOPS code for JA2 at 1.6 MPa and an initial temperature of 294 K compared to experiment.[29]

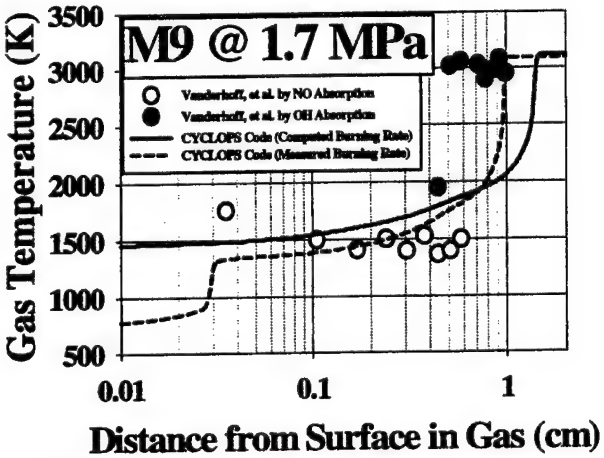

Figure 14. Flame-structure predictions of CYCLOPS for M9 at 1.7 MPa and an initial temperature of 294 K compared to experiment.[29] The dashed curve shows the temperature profile computed using the measured burning rate instead of the calculated burning rate as input.

the rapid temperature rise associated with the visible (secondary) flame are very well predicted. The

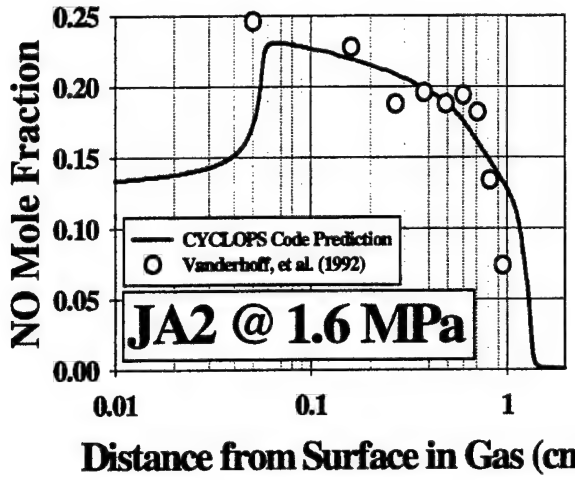

Figure 15. NO-profile prediction by CYCLOPS for JA2 at 1.6 MPa and an initial temperature of 294 K compared to experiment.[29]

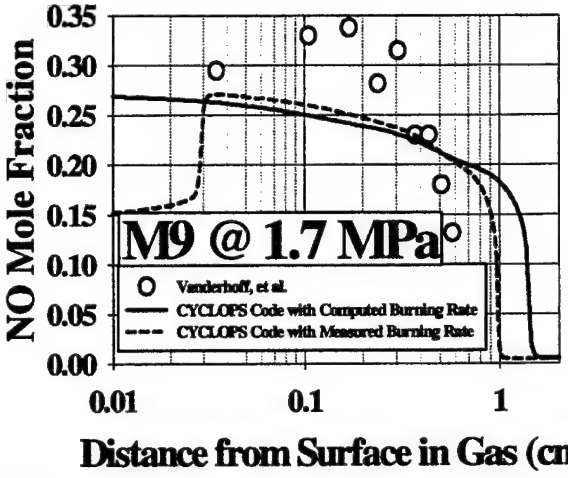

Figure 16. NO-profile predictions by CYCLOPS for M9 at 1.7 MPa and an initial temperature of 294 K compared to experiment.[29] The dashed curve shows the NO profile computed using the measured burning rate as input instead of the calculated burning rate as input.

NO mole-fraction profile is also very well predicted for JA2 as shown in Figure 15. The maximum mole fraction of NO is under-predicted for M9 (Figure 16) by about 25% although the agreement for the position of rapid drop off is good. In Figures 14 and 16 dashed curves illustrate how the theoretical profiles change if the measured burning rate instead of the computed burning rate is used as input. This was done only in these two figures to see how strongly the difference between measured and computed burning rate affects the agreement between theory and experiment. It is evident that much of the disagreement can be attributed to inaccuracies in the burning-rate calculation and not so much the reaction mechanism. Another useful comparison is between the previous measurements of the chemical species in the dark zone of double-base propellants and those predicted by the code. Table 4 has been abstracted from Vanderhoff et al.[14] with the addition of the CYCLOPS mole fraction predictions. All of the measurements are for a "hot" double-base propellant (i.e., one with high NG content) at about the same pressure. The CYCLOPS-computed dark-zone mole fractions were all taken at a distance from the surface of 0.1 cm for the comparable M9 propellant. Agreement between predictions for most of the species and their respective mole fractions is outstanding. Note that N_2 is the only species for which a significant difference occurs. The predictions, Figure 18, indicates N_2 rises to about 0.3 mole percent halfway through the dark zone. The measurements may be more representative of conditions at this point, so the agreement even for N_2 is good. Thus, it appears that the model gives a very credible account of the gas-phase processes, at least insofar as we have been able to test it.

Table 4. Comparison of measured dark-zone temperatures and mole percents for a double-base propellant similar to M9 to those computed by CYCLOPS (values taken at 0.1 cm). Experimental values and references are taken from Vanderhoff et al.[14]

Parameters	Heller & Gordon (1955)	Lengelle et al. (1984)	Vanderhoff et al. (1991)	CYCLOPS (present calc.)
P (MPa)	1.6	0.9	1.6	1.7
TDZ (K)	1600	1500	1500	1543
NO	24 %	21 %	24 %	25 %
CO	33	38		32
H_2	8	8		8
N_2	4	2		0.4
H_2O	20	20		19
CO_2	10	9		10
HCN	0.4			0.4
CH_4	0.8	2.6		0.9
C_2H_4	0.8	0.8		0.1

It is of interest to examine the major gas-phase species profiles for several of the propellants studied. Figure 17 shows the major species profiles for JA2 at 1.6 MPa and Figure 18 shows the corresponding case for M9 at close to the same pressure on the same scale.

9. Investigations of the Detailed Gas-Phase Chemistry

It is of interest to determine how the detailed chemistry has led to the predictions of CYCLOPS. This could lend insight, for example, into what types of ingredients might be used to affect the burn rates in some desired manner. As a crucial aid in this effort, we use postprocessing codes written over about the last 10 years for use with PREMIX, namely PREAD, ChemPlot, and

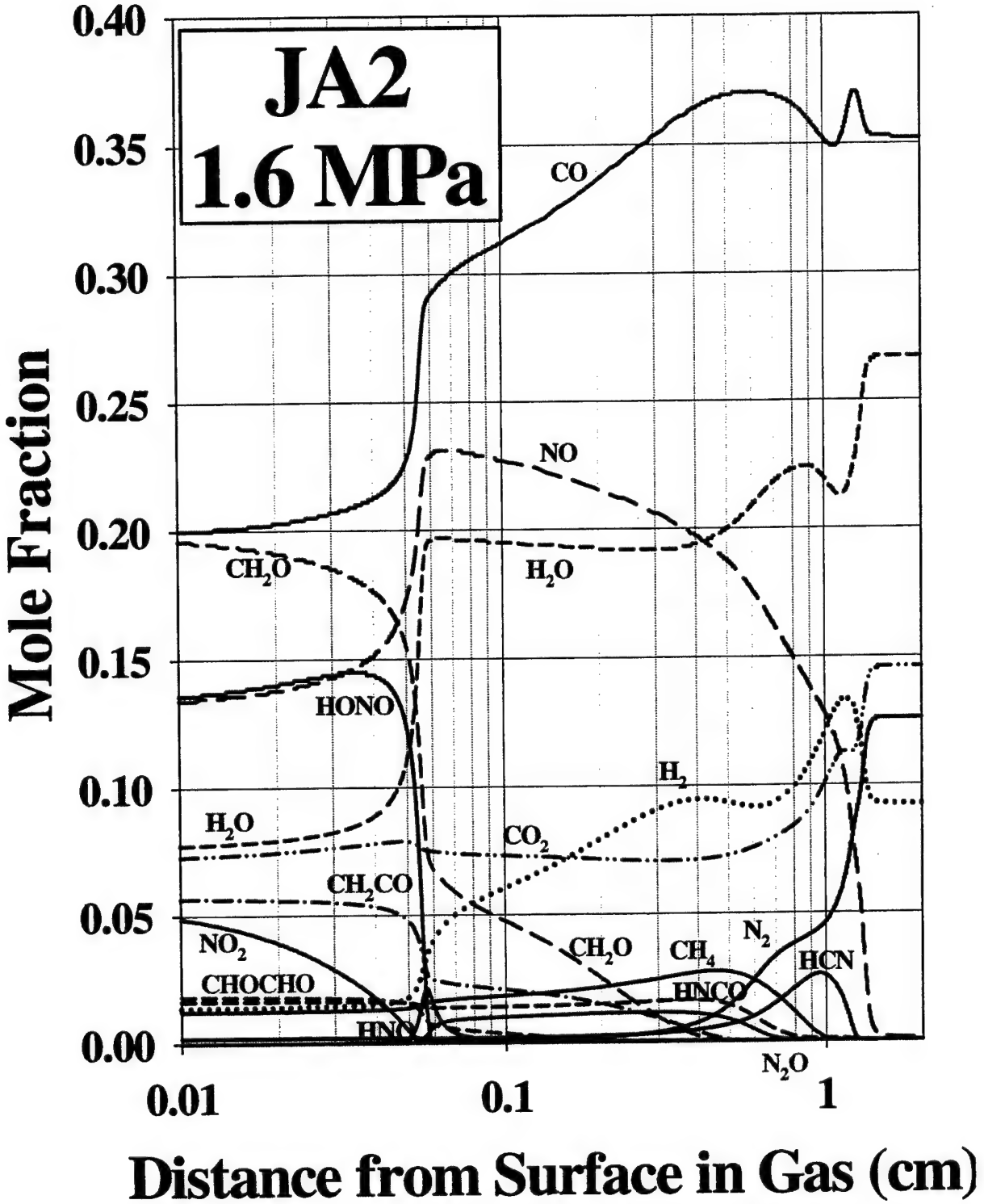

Figure 17. Major gas-phase species profiles predicted by the CYCLOPS code for JA2 at 1.6 MPa and an initial temperature of 294 K.

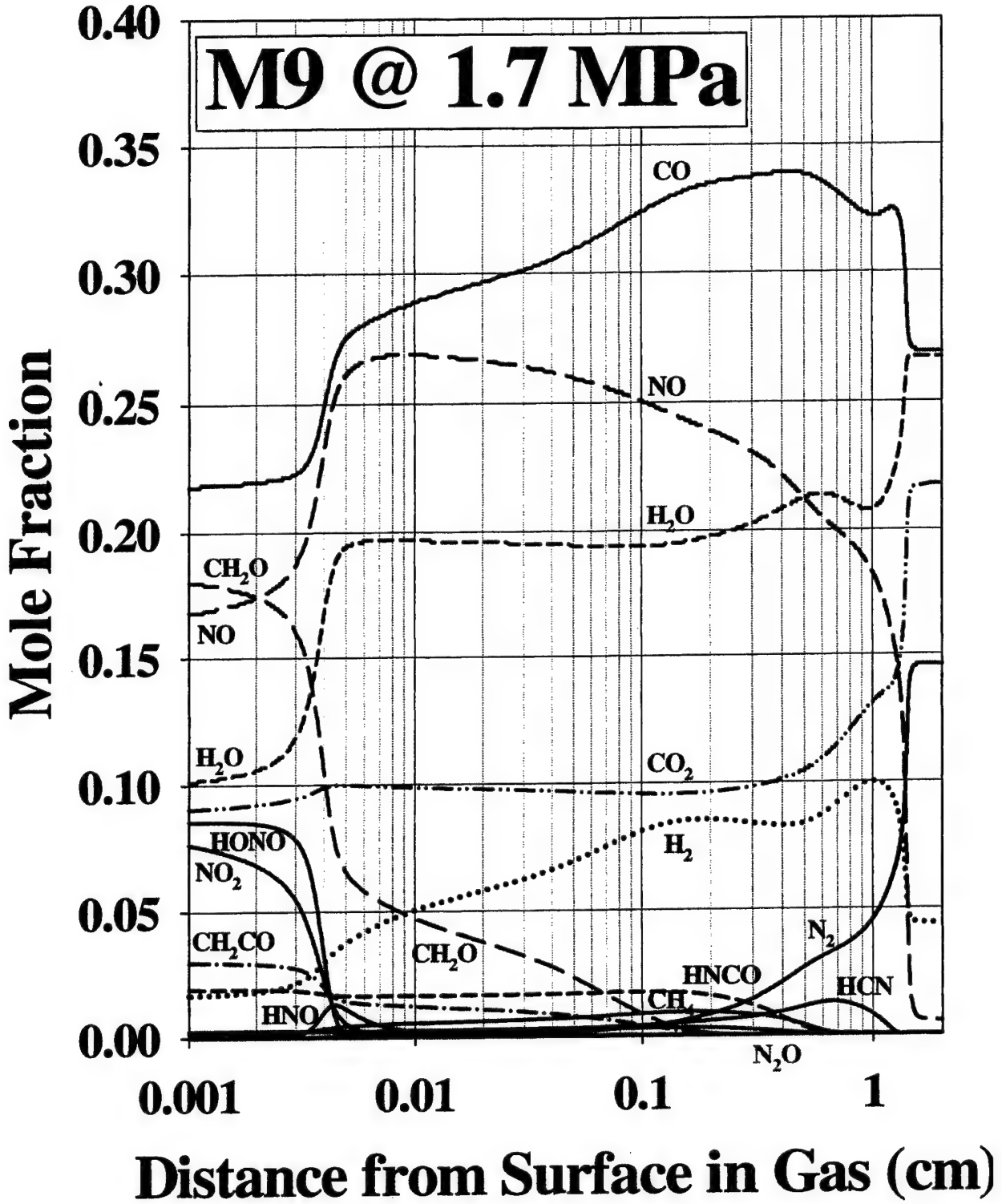

Figure 18. Major gas-phase species profiles predicted by the CYCLOPS code for M9 at 1.7 MPa and an initial temperature of 294 K.

Elemap.[34,35,36] These codes provide (1) an ASCII output file of many types of information including physical information (heat capacity, heat release rates, density, average molecular weight), and chemical information (sorted rates and sensitivities of individual species and temperature to the various reactions, and a pathways table which quickly shows the species reactive flow for a chosen element), (2) the ability to quickly obtain plots of a large variety of information, including the solution variables (species and temperature profiles), and (3) the ability to very rapidly obtain a pathways diagram. The codes have been invaluable in providing the understanding presented herein. As examples, we present details of how a slight inflection in the burning rate vs. pressure plot for M10 arises from changes in the key steps in the near surface gas phase chemistry, and we discuss and compare the dark zone chemistry for two of the propellants. These examples barely begin the investigations which could be done.

9.1 M10 Burning-Rate Pressure Dependence

Though the inflection in the M10 burning-rate curve near 100 atm is only rather slight, the fact that the experimental and predicted results agree so well suggests that it is real (see Figure 5). It would be of value to determine what consequences such an inflection might have on interior-ballistic calculations beyond those based on the usual simple fit to the $r = aP^n$ law. It is of immense interest to understand nonlinear burning rate plots such as this. For example, the inflection hints of the beginnings of a plateau region. For certain applications, as in rockets, it can be desirable to obtain long plateau regions since they can reduce the pressure dependence and, thus, the possibility of pressure induced oscillations.

We have carefully considered the inputs concerned in the present calculations. It is difficult to imagine that anything but variations in the key reactions in the gas-phase chemistry causes the modeling inflection, because all the other inputs vary more smoothly vs. pressure. The most important influence on the burning rate at any given pressure is the temperature profile (gradient and absolute value) just above the propellant surface. We have, from our PREAD postprocessing code, the capability of determining the reactions that have the greatest influence on the temperature just above the surface via sorting of the sensitivities computed using PREMIX. To that end, we present the temperature sensitivities for M10 at the second grid point, that is, the PREMIX-selected grid point just above the surface, for each of the selected pressures in Figure 5. The value of the temperature at this point, T_2, coupled with the surface temperature, is the most sensitive determinant of the computed heat feedback to the surface. Here, we present logarithmically normalized sensitivities,viz:

$$S_k = \frac{A_k}{T_m}\left(\frac{\partial T}{\partial A_k}\right) \tag{8}$$

where A_k is the A-factor of the kth reaction and T_m is the maximum temperature in the calculational domain. The important points here are that T_m is a constant value (usually not the adiabatic

temperature, because, to obtain accurate burning rates, the calculational domain may generally be cut off well below the point where that is reached), and multiplication by A_k places the sensitivities on the same relative scale so the influence of the various reactions can be compared. The sensitivities for the 8 pressures are given in Appendix C. Along with the normalized sensitivities, we also present in the last column the value relative to the largest sensitivity for easy comparison. The lists are terminated at the top 20 sensitivity values or at the 5% level. For a given reaction, a positive sensitivity means an increase in the rate coefficient would result in an increase in T near the propellant surface, while a negative sensitivity means the opposite. Since the gradient in T would also increase for a positive sensitivity, and vice versa, it is to be expected that a positive sensitivity means an increase in the rate coefficient would generally cause an increase in *computed burning rate*, and vice versa. One must keep in mind that the reactions listed in Appendix C may have net rates in either direction; these net rates can even reverse at different points in the flame. Most of the reactions which appear in these lists have a noticeably high standing in the sorted rates lists for the species involved (not shown).

A few important points are noted in perusing the sensitivity tables preliminary to pointing out how the changing chemistry vs. pressure produces the inflection. First, many of the reactions highest in the lists, i.e., most important to determining the heat feedback, involve radical species assumed to be produced in the surface products. Of these radical reactions, many are recombinations that release a lot of heat. An example is R358, CH_2CO (+M) = CH_2 + CO (+M), which is nearly 100% reversed. These are the primary chemical drivers of the heat into the propellant surface. Some of them, e.g. R347, HCO + NO_2 = CO + HONO, and R348, HCO + NO_2 = H + CO_2 +NO, proceed in the forward direction, indicating two different product sets for the same reactants. This particular pair of reactions is high on the sensitivity lists and with opposite signs probably because R348 is radical neutral, while R347 destroys a radical chain-carrying center.

At the lowest pressures (see, e.g., the 0.3-MPa table), we note T_2 is primarily influenced by R348, R358, R197, R333, R347, etc. R3, the three-body reaction H + NO (+M) = HNO (+M) whose rate is highly pressure dependent, is fairly far down the list. As the pressure increases to about 3 to 10 MPa, the rate of R3 increases faster, relative to the bimolecular reactions, so it is not surprising that its sensitivity also climbs higher on the sorted list at these pressures. Either R21, HNO + NO_2 = HONO + NO, or R161, H + HNO = H_2 + NO, rapidly follow R3, so that the sequence of R3 followed by R21 or R161 leads to a modest radical loss. (R21 and R161 are very fast and not rate determining in this sequence, explaining why R3 is higher on the sensitivity list. We believe this is why the slope in the burning rate curve decreases.

At 30 MPa, R19, HNO + NO = N_2O + OH, and R166, HNO + HNO = N_2O + H_2O, first begin to make their presence in the mechanism known near the surface. Their influence, especially that of R19, increases with increasing pressure until at 1000 MPa, R19 is at the top of the list. It is likely these reactions grow in importance because higher pressure causes R3 to increasingly favor a larger [HNO], and, for R19 which has a fairly large activation energy of 29 kcal/mole, the higher temperatures observed near the surface as the pressure increases (not shown) will cause the rate of

the reaction to greatly increase. Thus, the sensitivity lists indicate these reactions cause the gradient in the burning rate curve to increase at pressures above 30 MPa.

The strong influence of R19 and R166 on the combustion at pressures above 30 MPa is one of the greatest surprises in this work. Strong evidence has been given in prior works establishing that these reactions are of central importance in controlling the structure (length) of nitrate-ester-propellant dark zones, especially R19 which is the primary radical source that causes the rather dormant mixture to re-ignite and the secondary flame to form.[14,15,16,17] At pressures of 10 MPa and below, this reaction has a negligible rate near the propellant surface. As the pressure increases, we find that the secondary flame, not surprisingly, moves closer to the propellant surface (not shown). At the highest pressures, there in fact is no dark-zone plateau discernable at all in the temperature profile; even so, the "dark-zone reactions" (R19 & R166) still occur at higher pressures, and have a high sensitivity ranking. Detailed analysis shows that the rate of these reactions is negligible very close to the propellant surface, even at 1000 MPa, so the reason for their high sensitivity rankings is not obvious on that basis.

The physico-chemical basis for the increased sensitivity of the burning rate to the dark-zone reactions may be further understood by comparing details of the results at two extreme pressures, 1 and 1000 MPa. The concept of characteristic distance for heat transfer in the near surface region[37] is helpful here. One can express the heat feedback to the surface in terms of the net volumetric heat release from the gas-phase reactions, $q(x)$, by the following simple expression (valid for constant specific heat c_p and thermal conductivity λ_g)

$$\lambda_g\left(\frac{\partial T}{\partial x}\right)_{x=0^+} = \int_0^\infty q(x) e^{-\frac{\dot{m}c_p}{\lambda_g}x}\, dx \qquad (9)$$

This expression shows that the heat released at some distance x from the surface contributes to the total heat feedback with exponentially diminshing effectiveness the larger x is relative to the characteristic distance, $\lambda_g/\dot{m}c_p$. We have computed the characteristic distances for the M10 flames to be about 5.5×10^{-4} cm at 1 MPa and 8.6×10^{-6} cm at 1000 MPa. Temperature and mole-fraction plots for a few key species are given in Figures 19 and 20. The key feature to look for in these profiles is the distance at which the NO mole fraction peaks, signaling the end of the first reaction stage involving NO_2 and HONO reduction. At 1 MPa (Figure 20), there is subsequently a delay in the reduction of NO to final product N_2. This delay is the primary reason for the formation of the dark zone, indicated by the various profiles to be in the region from 0.15 to 1 or 2 cm. The end of the first stage clearly occurs at about 0.15 cm, which is very large compared to the characteristic distance. Thus, the visible flame reactions, which succeed the dark-zone reactions, play no role in the heat feedback at this pressure.[§] At 1000 MPa (Figure 19), the profiles do not indicate the

[§] The dark-zone flame structure and chemistry in the case of M10 at 1 MPa is very similar to that of JA2 at 1.6 MPa, including similar concentrations of trace carbon-containing species and the hump in some of the profiles at midpoint of the dark zone; except that the dark zone is,

existence of a separate dark-zone region because, in this case, the dark-zone reactions are greatly accelerated due to the higher temperature and pressure. Thus, the dark-zone reactions no longer act as a slow, spatially extended bottleneck for creating the radicals responsible for releasing the heat of the visible flame. Since at this pressure the characteristic distance is larger than the distance at which the NO begins to disappear, some of the energy release associated with the visible flame contributes to the heat feedback. This explains the high sensitivity rankings of R19 and R166 (and also R341, R181, and R149, which are associated with trace dark-zone species).

It previously had been thought by most workers (including us) that the chemistry responsible for the formation of dark zones at low pressure cannot affect the burning rates of propellants. This belief was based on the argument that, at low pressures, this chemistry keeps the secondary-flame energy release remote from the surface, and at high pressures the dark zones are not perceptible in photographs, presumably meaning that the "dark-zone chemistry" is no longer relevant. ***Our analysis of the reactions critically determining the high-pressure burning rate show that this chain of reasoning is, in fact, wrong. The reactions causing the formation of dark zones at low pressure are extremely important to the burning rate at high pressure.*** Since this chemistry has not been very well-established, especially for nitramine propellants, it is important for it to receive renewed attention.

9.2 Dark-Zone Structure in JA2 and M9

One of the more curious features often observed in the flame structures of combusting propellants at low pressure (less than approximately 100 atm) is the formation of a dark zone (DZ), a non-luminous region between the condensed phase propellant and the high-temperature luminous flame zone. The discussion on M10 in the last section indicates DZ chemistry may become extremely important to the propellant burning rate at high pressures; and, the chemistry of this feature is of technical interest in its own right. Therefore the DZ chemistry observed in this work is discussed here in more detail.

As pointed out in the earlier discussion of flame structure, our computations at about 1 – 2 MPa predict the formation of dark zones for JA2, M9, and M10 (computations for M2 were not performed at large distances; it undoubtedly also does form a DZ). This result is evidenced by the appearance of near-plateau regions in the various concentration and temperature profiles. For example for JA2, from the temperature profile in Figure 13, the DZ at 1.6 MPa extends from the end of the first stage combustion, 0.055 cm, to about 1.3 cm where the sharp upwards temperature gradient indicates that the runaway in the second stage chemistry to final equilibrium occurs. It is well known in the case of nitrate ester propellants that DZs form because of the conversion of NO_2 and HONO near the propellant surface to NO, and that the intermediate NO is a slowly reacting oxidizer which retards the chemistry.[14,15,16,17] The end of the DZ, signified by rapid conversion of the

---

not surprisingly, longer at this lower pressure. The chemistry of the JA2 dark zone is considered in more detail and compared with M9 in the next section.

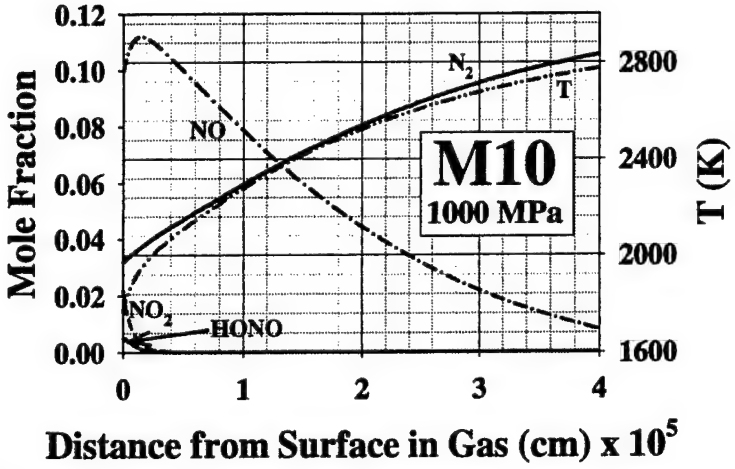

Figure 19. Key species profiles defining the dark zone along with the temperature profile for M10 at 1000 MPa. The end of the primary reaction zone coincides with the final consumption of NO_2 and HONO to produce NO.

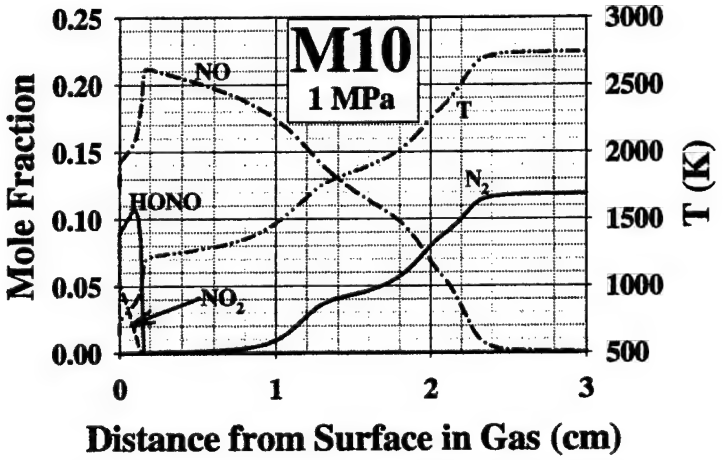

Figure 20. Key species profiles defining the dark zone along with the temperature profile for M10 at 1 MPa. The end of the primary reaction zone coincides with the final consumption of NO_2 and HONO to produce NO. The end of the dark zone is defined by the reduction of NO to N_2.

intermediates to final products with a rapid temperature rise, occurs due to the build-up of heat and, especially, radical concentrations. Though the DZ was intriguing to early researchers, it's existence can be simply explained as the result of a delayed chemical ignition of the second reaction stage due

to the presence of comparatively unreactive intermediates. (NO is the unreactive intermediate in the case of nitrate-ester propellants, NO and HCN in the case of nitramine propellants. Note that ignition delays in chemistry upon formation of a hot gaseous mixture are not at all unusual; they are frequently observed, especially in shock tube experiments. The challenge in the case of propellants is to determine the correct chemistry for a rather complicated mixture with rather scant experimental information available about the exact conditions at leading edge of the DZ.) The primary constituents of the DZ for nitrate esters are H_2, NO, CO, CO_2, N_2, and H_2O (see, e.g., Figures 17 and 18 and Table 4). In general, the concentrations of the first three species are above equilibrium values, while the latter three are below. At the runaway point, conversion of the first three to final products occurs. A simplified kinetic scheme[14,16,17] indicates that R19, HNO + NO = N_2O + OH, is the primary source reaction for radical buildup in the case of nitrate esters. Thus the DZ length is quite sensitive to the rate coefficient chosen for R19. At the end of the DZ, where the final steep temperature gradient occurs, the remaining NO is converted to final product N_2, mostly via R165, NO + H = N + OH, followed rapidly by R163, N + NO = N_2 + O; some of the CO is converted to CO_2 via R44, CO + OH = CO_2 + H, and some of the H_2 is converted to H_2O via R52, O + H_2 = OH + H, followed by R50, OH + H_2 = H_2O + H.

One feature in common to the temperature profiles that is surprising is the presence of a slight hump about halfway through the DZ. These humps are most prominent in the 1.6 MPa JA2 profile at 0.7 cm (Figure 13) and the 1.0 MPa M10 profile at 1.3 cm (Figure 20). There is a more modest one in the 1.7 MPa M9 profile at 0.5 cm (Figure 14). Although such a hump is not readily discerned in most experimental profiles, it is a rather small feature that would not be easy to observe. Example figures and photographs of burning propellants given in the literature and presentations frequently have been carefully chosen to illustrate the qualitative features of the phenomenon, especially the DZ. What is frequently not pointed out in various still-picture examples is that there is almost always a fairly large amount of flicker in the flame position. This may have contributed to the overlap in temperature regions at the end of the JA2 and M9 DZs in the experimental results of Figures 13 and 14. The measurements were made using absorption spectroscopy on NO and OH, which are primarily present in the intermediate (DZ) temperature and high temperature spatial regions, respectively. The measurements indicate the intermediate temperatures extend to about 0.2 cm larger distances than those at which the high temperatures begin! The problem with flickering can also be compounded with reproducibility (the NO and OH results were from different runs) and spatial resolution difficulties. Thus, the lack of a hump in experimental profiles cannot necessarily be taken as evidence against the present prediction of a modest hump. Evidence for the presence of such a hump is found in the temperature profile taken at 5.0 MPa for the double base propellant "N-powder" in the work of Zenin.[38]

Since the major reactions controlling the DZ behavior were already discussed in the last paragraph, in the remainder of this section we discuss the predicted chemistry of the trace DZ species, and compare the results for JA2 and M9. (Though the modeling was done at slightly different pressures, taken to match the available experiments, these are close enough to make comparisons reasonable.) It should be pointed out that, as we will discuss further below, the hump primarily arises from reactions of trace species that are present at the leading edge of the DZ. One

could have a concern here that some of the trace species predicted are the result of our assumed condensed phase products for the various ingredients, and that these may not be unique; in other words, the question arises whether the entire idea may be incorrect and the effort here to investigate the associated chemistry is wasted. However, predicted and observed DZ-species concentrations (see Table 4) are quite close even for most of the trace species. These similarities, especially that of CH_4, which we will see is very important in this discussion, suggest the associated chemistry and predicted consequences to the temperature profile are at least qualitatively correct.

Intermediate trace species predicted in the DZs of JA2 at 1.7 MPa and M9 at 1.6 MPa include CH_4, HCN, HNCO, N_2O, HNO, CH_2O, and CH_2CO; and HCNO. The first seven of these are shown in Figures 17 and 18 and are present at the level of several mole percent. The species CH_2O and CH_2CO are the primary fuels in the first stage. CH_2CO is formed near the surface, primarily from the rapid recombination of CH_2 with CO (R358), while CH_2O is present as a condensed phase product. In the first stage, most of the CH_2O and CH_2CO react, globally, with NO_2 and HONO oxidizers, yielding H_2, H_2O, CO, and the less reactive NO oxidizer. A few percent of the CH_2O and CH_2CO fuels remains from this rich mixture. CH_4 comes from the condensed phase (see Table 3), and is formed early in the first stage via R310, $CH_3 + CH_2O = CH_4 + HCO$, and early in the DZ by -R222, $CH_3 + H_2 = H + CH_4$. It is important to note that the CH_3 formed early in the DZ arises from consumption of part of the leftover CH_2CO via R365, $CH_2CO + H = CH_3 + CO$. Thus, all of CH_2, CH_3 and CH_4 coming from the condensed phase can directly or indirectly contribute to CH_4 observed in the DZ.

Note that at the point of sharp gradients dividing the first and second stages (0.055 cm for JA2, 0.0045 cm for M9) there is a sudden, sharp peaking in the concentration of HNO to about 1 or 2 mole percent. HNO is formed at this point primarily by R197, HCO + NO = HNO + CO. However, we have been unable to discern why the HNO profile is so strongly peaked and what controls its maximum concentration. The HNO concentration apparently controls the amount of trace N_2O formed at the leading edge of the DZ. N_2O is formed here as the HNO is consumed, primarily via R166, $HNO + HNO = N_2O + H_2O$. (We have found that the relative concentration of N_2O in M9 vs. JA2 DZs is roughly proportional to the square of the [HNO]. R166 is second order in HNO and the temperature difference between the two propellants at the end of the first stage is small, suggesting such a proportionality is to be expected.) A small portion of the N_2O formed at this point is due to R19, $HNO + NO = N_2O + OH$. R19 is also primarily responsible for the slight continuation of growth in $[N_2O]$ until its maximum partway through the DZ.

Traces of HCNO and HNCO are formed primarily early in the first stage via reactions of CH_2 with NO (R335 and R333, respectively). HCNO is converted to HNCO early in the DZ via R341, HCNO + H = H + HNCO, accounting for the slight increase in HNCO to its maximum value about midway through the DZ. At the same time as the HCNO is being consumed, the leftover traces of CH_2O are converted to CO and H_2. The leftover traces of CH_2CO are converted to CO, CH_2, and CH_3 via unimolecular reaction R358 and reaction with H atom, R365. As mentioned above, the CH_3 is rapidly converted temporarily to CH_4 via reaction with H_2 (-R222) and is one of the primary sources of the CH_4 in the DZ. The CH_2 rapidly reacts with NO to make more HNCO via R333.

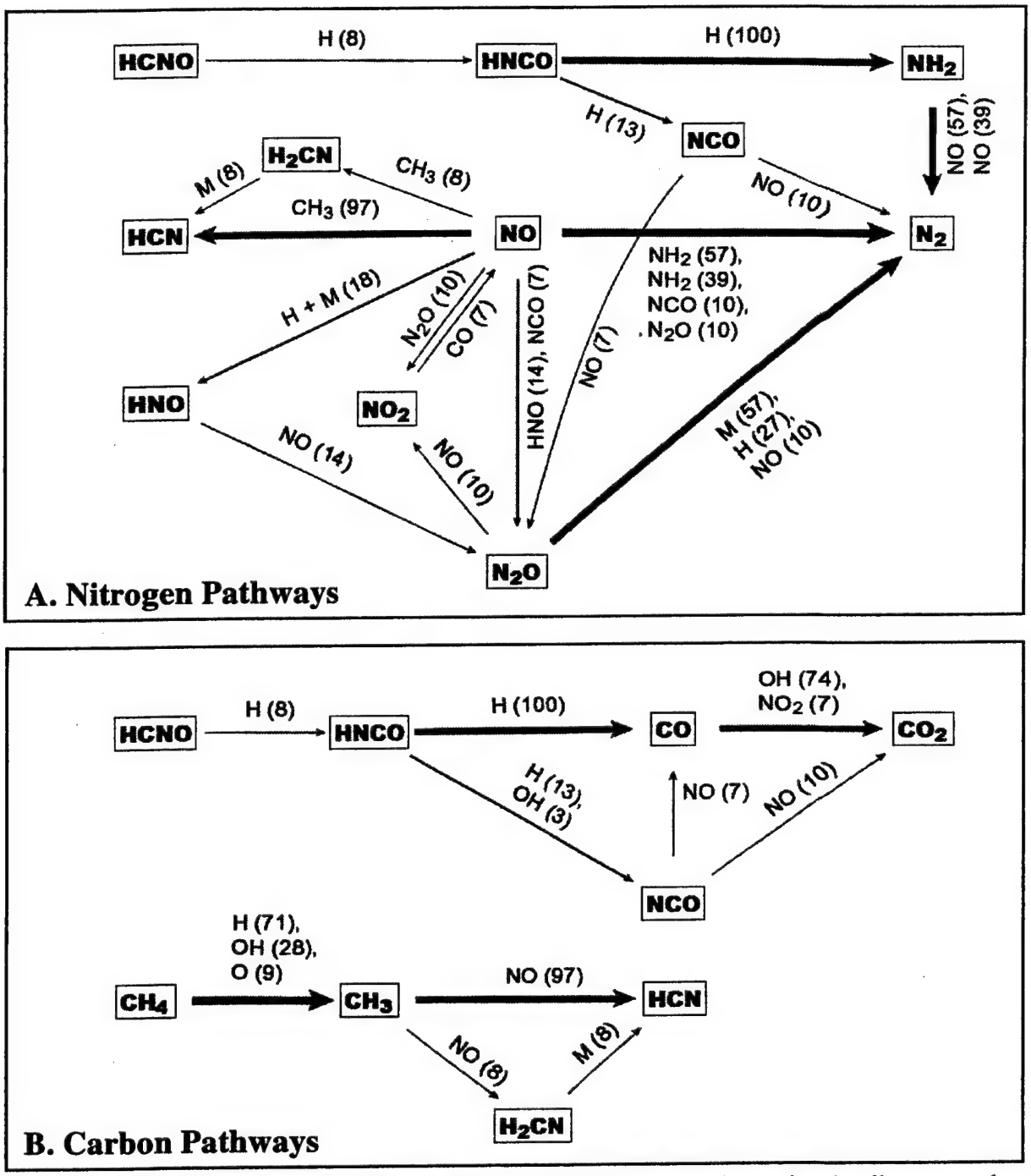

Figure 21. Pathway diagrams for chemistry of JA2 at 1.6 MPa in the region leading up to the hump in the DZ temperature profile at about 0.7 cm. The diagrams are based on relative rates of the chemical reactions integrated over the spatial coordinate from 0.5 to 0.75 cm (resulting in units of mole/cm^2-s prior to the normalization to 100). (a) Nitrogen species. (b) Carbon species. In both the nitrogen and carbon diagrams, the relative rate of 100 is 4.99×10^{-4} mole/cm^2-s; note that this refers to the reaction of HNCO with H in both cases.

After the consumption of CH_2O, CH_2CO, and HCNO, the CH_4, HNCO, and N_2O almost simultaneously begin to be consumed. This concerted process is the main source of the heat release and hump in the temperature profiles about midway through the DZs. Pathway diagrams for JA2 illustrate the chemical pathways connecting nitrogen and carbon containing species in this spatial region (see Figure 21). Consumption of CH_4 occurs primarily via H atom abstraction reactions with H and OH (R222 and R257) to form CH_3. R339, $CH_3 + NO = HCN + H_2O$, then rapidly occurs, as well as secondary reaction R340 temporarily forming H_2CN. HCN is a relatively stable intermediate because both bonds are strong. (Its C-H bond is, for example, about 20 kcal/mole stronger than the C-H bond in CH_4.) Like much of the NO, most of it therefore survives to the end of the DZ. HNCO reacts primarily via R181, $HNCO + H = NH_2 + CO$; some is diverted in a secondary path to NCO. The NH_2 thus formed rapidly reacts with NO: R149, $NH_2 + NO = N_2 + H + OH$, and R150, $NH_2 + NO = N_2 + H_2O$. (In the nitrogen pathways diagram, R149 is the one which is modestly faster.) N_2O is primarily consumed by R2, $N_2O (+M) = N_2 + O (+M)$, and R113, $N_2O + H = N_2 + OH$. (Note that R149 and R2, as well as R19, can contribute to radical buildup.) For JA2, the sorted heat releases indicate the primary exothermic reactions in this region are, in decreasing order of importance, R339, R150, and R113; these are slightly countered by the endothermic R2 whose heat consumption is roughly equivalent to the heat production of R113. For M9, similar analysis indicates R150 and R339 are, in order, the most important. (Although these reactions account for the bulk of the heat release, there are several other reactions whose heat releases are up to about half the size of the smallest of these.) Pathway diagrams (not shown) in the region leading up to the M9 hump are similar to those for JA2, except that CH_4, CH_3 and N_2O reactions are much less important relative to HNCO reactions.

We are now in a position to explain the relative sizes of the humps in the JA2 and M9 temperature profiles. CH_4 and HNCO are the main species whose reactions produce the heat that gives rise to these humps. Recounting the above, CH_4 arises (1) directly from the assumption of its production from the condensed phase, (2) from CH_3 reaction with CH_2O in the first stage, and (3) from temporary conversion of CH_2 in the first stage to CH_2CO, followed early in the DZ by the sequence $CH_2CO \rightarrow CH_3 \rightarrow CH_4$. HNCO arises (1) directly from $CH_2 + NO$ near the surface and (2) by $CH_2 + NO$ production of HCNO near the surface followed by conversion of HCNO to HNCO at the leading edge of the DZ. The trace concentrations of CH_4 and HNCO species, which ultimately give rise to the humps in the respective temperature profiles, are larger for JA2 than for M9. Thus, the hump is more pronounced for JA2 than for M9 (See Figures 17 and 18). Finally, the reason concentrations of CH_4 and HNCO are larger for JA2 may be understood by perusal of Table 3. The CH_4, CH_3, and CH_2 concentrations, produced from the condensed phase reactions and which lead to CH_4 and HNCO, are all larger for JA2 than for M9. (Similar observations also apply to M10, which produces the relatively pronounced hump in Figure 20. Although the model assumes no CH_4 or CH_3 are produced from the condensed phases, there is a relatively large amount of CH_2. CH_2, as discussed above, can lead to HNCO and CH_4 production in various portions of the flame and their ultimate consumption in the DZ.)

10. Conclusions

The current state of the art in energetic-material combustion modeling could be described as one of frustrated opportunity. On the one hand, great progress has been made in developing credible elementary reaction mechanisms for the gas phase; on the other hand, progress in describing condensed-phase and surface processes has been far less than commensurate. The approach embodied by the CYCLOPS code takes full advantage of the availability and present possibility of good elementary-reaction gas-phase mechanisms while offering a viable strategy for dealing quantitatively with the unknown mechanics of subsurface reaction and surface regression through the agency of the pyrolysis law. The link between the pyrolysis law of mass regression and the detailed chemistry of the gas phase is effected by hypothesizing the condensed-phase decomposition products in number and kind consistent with atomic balance and available experimental results. Although our present approach is clearly an interim solution waiting for a comprehensive treatment of the burning-surface and condensed-phase processes, there are a number of features in its favor. Burning rate often is not a sensitive function of the underlying submodels. CYCLOPS exploits this insensitivity since small imperfections in the decomposition-product set for any one ingredient may not seriously degrade the calculated burning rate for the whole multi-ingredient propellant.

Another favorable feature of our approach is the generality of its assumptions. The pyrolysis law has been found to provide a good empirical description of both reactive and evaporative surface regression mechanisms. (Evaporative mechanisms for ozone and RDX are discussed by Miller and Anderson.[2]) The set of decomposition products for each ingredient used in this study may well not be optimum, but they can be easily changed as new research results become available. Apart from the potentially imprecise assumption that the ingredients decompose (in the condensed phase) independently of each other, the approach taken here *must* work if the combustion is one-dimensional, the pyrolysis law is valid, the decomposition products correct, and the gas-phase reaction mechanism complete and accurate. Of course, the accuracy of the predicted burning rate will also be a function of the accuracy of other input data, such as the ingredient and propellant-amalgam heats of formation, that even a hypothetically rigorous model would require as well. Thus, CYCLOPS is a flexible vehicle for making practical calculations of the formulation dependence of burning rate while incorporating evolving improvements in mechanistic understanding. *It should be borne in mind that the model does not have to be perfect to be useful; it would be enormously helpful to have even semi-quantitatively correct theoretical guidance in propellant-formulation work.*

Finally, even if molecular-dynamic simulations of the condensed-phase and surface-regression phenomena should become routine and reliable, the calculational model proposed here may well be the most practical way of coupling those results with the present rigorous continuum-mechanics description of the gas phase in order to predict burning rates.

11. References

1. Miller, M. S., B. M. Rice, A. J. Kotlar, and R. J. Cramer. "A New Approach to Propellant Formulation: Minimizing Life-Cycle Costs Through Science-Based Design." *Clean Products and Processes*, vol. 2, pp. 37–46, 2000.

2. Miller, M. S., and W. R. Anderson. "Energetic-Material Combustion Modeling With Elementary Gas-Phase Reactions: A Practical Approach." Chapter 2.12 in *Solid Propellant Combustion Chemistry, Combustion, and Motor Interior Ballistics*, V. Yang, T. B. Brill, and W. Z. Ren, (eds.), *Progress in Astronautics and Aeronautics Series* vol. 185, AIAA, New York, pp. 501–531, 2000.

3. Zenin, A. "HMX and RDX: Combustion Mechanism and Influence on Modern Double-Base Propellant Combustion." *Journal of Propulsion and Power*, vol. 11, pp.752–758, 1995.

4. Kee, R. J., J. F. Grcar, M. D. Smooke, and J. A. Miller. "A Fortran Program for Modeling Steady Laminar One-Dimensional Premixed Flames." SNL Report SAND85-8240, December 1985, reprinted, Sandia National Laboratories, Albuquerque, NM, March 1991.

5. Miller, M. S., and T. P. Coffee. "On the Numerical Accuracy of Homogeneous Solid Propellant Combustion Models." *Combustion and Flame*, vol. 50, pp. 75–88, 1983.

6. Leider, H. R., and D. L. Seaton. "Nitrate Ester Decomposition and Degradation of Molecular Weight in Nitrocellulose from Thermal Decomposition of PBX-9404 Below 100C." Lawrence Livermore Laboratory Report UCRL-52776, Livermore, CA, May 8, 1979.

7. Gelernter, G., L. C. Browning, S. R. Harris, and C. M. Mason. "The Slow Thermal Decomposition of Cellulose Nitrate." *Journal of Physical Chemistry*, vol. 60, pp. 1260–1264, 1956.

8. Bunte, S. W., and M. S. Miller. "Atomistic Simulations of the Physical Properties of Nitrate Esters." Army Research Laboratory Technical Report ARL-TR-2496, U.S. Army Research Laboratory, Aberdeen Proving Ground, MD, May 2001.

9. Todd, J., and W. G. Glasser. "NMR Spectroscopy of Nitrocellulose Samples." Section IV in Wolfgang G. Glasser and Audrey G. Zink's, "Final Report on Cellulose and Cellulose Nitrate Characterization." Contract Report to AlliantTechSystems, Inc., Radford, VA performed at Virginia Polytechnic Institute and State University, Blacksburg, VA, February 1996.

10. Taylor, J., C. R. L. Hall, and H. Thomas. "The Thermochemistry of Propellant Explosives." *Journal of Physical and Colloid Chemistry*, vol. 51, pp. 580–592, 1947.

11. Miller, M. S., and A. J. Kotlar. "Thermal Transport Properties of Solid Gun Propellants." *Proceedings of the 29th JANNAF Combustion Meeting, Chemical Propulsion Information Agency*, Publication 593, vol. 1, pp. 149–159, 1992.

12. Vladimiroff, T., Y. P. Carignan, D. S. Chiu, and A. K. Macpherson. "The Development of a User Friendly Thermodynamic Code for the Personal Computer." *Proceedings of the 24th JANNAF Combustion Meeting, Chemical Propulsion Information Agency*, Publication 476, vol. II, p. 39, 1987.

13. Vladimiroff, T., Y. P. Carignan, D. S. Chiu, and A. K. Macpherson. "Flame Temperature Calculations at High Temperature and Pressure." Propellants, Explosives and Pyrotechnics, vol. 19, p. 281, 1994.

14. Vanderhoff, J. A., W. R. Anderson, and A. J. Kotlar. "Dark Zone Modeling of Solid Propellant Flames." *Proceedings of the 29th JANNAF Combustion Subcommittee Meeting, Chemical Propulsion Information Agency*, Publication No. 593, vol. II, p. 225, 1992.

15. Anderson, W. R. "The Chemical Mechanism of H_2/NO Combustion at Intermediate Temperatures and Its Relation to the Dark Zone of Propellants." *Proceedings of the 30th JANNAF Combustion Meeting, Chemical Propulsion Information Agency*, Publication 606, vol. II, p. 205, 1993.

16. Anderson, W. R., N. Ilincic, N. E. Meagher, K. Seshadri, and J. A. Vanderhoff. "Detailed and Reduced Chemical Mechanisms for the Dark Zones of Double Base and Nitramine Propellants in the Intermediate Temperature Regime." *Proceedings of the 32nd JANNAF Combustion Subcommittee Meeting and 1995 Propulsion Systems Hazards Subcommittee Meeting*, Joint Sessions, CPIA Publication 638, vol. I, p. 197, 1995.

17. Ilincic, N., W. R. Anderson, K. Seshadri, and N. E. Meagher. "Simplified Chemical-Kinetic Mechanisms for Characterizing the Structure of the Dark Zones of Double Base and Nitramine Propellants." *Twenty-Sixth Symposium (International) on Combustion* (The Combustion Institute, Pittsburgh, PA), vol. II, p. 1997, 1996.

18. Bowman, C. T., R. K. Hanson, D. F. Davidson, W. C. Gardiner, Jr., G. P. Lissianski, G. P. Smith, D. M. Golden, M. Frenklach, and M. Goldenberg. GRI Mech Version 2.11, Internet Address: <http://www.me.berkeley.edu/gri_mech/>.

19. Diau, E. W., M. J. Halbgewachs, A. R. Smith, and M. C. Lin. "Thermal Reduction of NO by H2: Kinetic Measurement and Computer Modeling of the HNO + NO Reaction." *International Journal of Chemical Kinetics*, vol. 27, p. 867, 1995.

20. Anderson, W. R., "Heats of Formation of HNO and Some Related Species." *Combustion and Flame*, vol. 117, p. 394, 1999.

21. Juhasz, A. A., (ed.), "Round Robin Results of the Closed Bomb and Strand Burner." CPIA Publication 361, *Chemical Propulsion Information Agency*, Columbia, MD, July 1982

22. Miller, M. S., U.S. Army Research Laboratory, Aberdeen Proving Ground, MD, 1985–1993, unpublished data.

23. Atwood, A. I., C. F. Price, P. O. Curran, and N. G. Zwierzchowshi. "Burning Rate, Radiant Ignition, and Global Kinetics of a Nitrocellulose Propellant." *25th JANNAF Combustion Meeting*, CPIA Publication 498, vol. I, *Chemical Propulsion Information Agency*, Columbia, MD, pp. 69–81, 1988.

24. Andreev, K. K. "Experimental Investigation on Combustion of Explosives." *Collection of Articles on Theory of Explosives*, Oborongiz, Moscow, pp. 39–65, 1940.

25. Andreev, K. K. *Thermal Decomposition and Combustion of Explosives*, Gosenergoizdat, Moscow-Leningrad, 1957.

26. Andreev, K. K., A. P. Glazkova, and I. A. Tereshkin. "Investigation of Pressure, Temperature, and Density Influence on Combustion, Explosives, and Some Composites." Chemical Physics Institute, Moscow, 1959, 1960.

27. Kondrikov, B. N., V. M. Raikova, B. S. Samsonov. "On Kinetics of Combustion of Nitrocompounds at High Pressure." *Fizika Goreniya i Vzryva*, no. 1, pp. 84–90, 1973.

28. Grollman, B. B., and C. W. Nelson. "Burning Rates of Standard Army Propellants in Strand Burner and Closed Chamber Tests." BRL-MR-2775, U.S. Army Ballistic Research Laboratory, Aberdeen Proving Ground, MD, August 1977.

29. Vanderhoff, J. A., M. W. Teague, and Anthony J. Kotlar. "Absorption Spectroscopy through the Dark Zone of Solid Propellant Flames." BRL-TR-3334, U.S. Army Ballistic Research Laboratory, Aberdeen Proving Ground, MD, April 1992.

30. Kirkpatrick, D. W. Propellant Description Sheet for M9, DA Lot Number RAD-PE-792-77, Radford Army Ammunition Plant, Radford, VA, 16 April 1990.

31. Juhasz, A., C. Bullock, B. Homan, and D. Devynck. "Micro Closed Bomb for Characterizing the Burning of Propellants at Gun Pressures." *36th JANNAF Combustion Subcommittee Meeting*, CPIA Publication 691, vol. 1, pp. 175–187, October 1999.

32. Zenin, A. A., and O. I. Nefedova. "Burning of Ballistite Powder over a Broad Range of Initial Temperatures." *Fizika Goreniya i Vzryva*, vol. 3, pp. 45–53, 1967.

33. Eisenreich, N., W. Eckl, T. Fischer, S. Weiser, G. Langer, A. Baier. "Burning Phenomena of the Gun Propellant JA2." *Propellants, Explosives, Pyrotechnics*, vol. 25, pp. 143–148, 2000.

34. Anderson, W. R., S. W. Haga, J. F. Nuzman, A. J. Kotlar, and R. J. Anderson. PREAD Computer Code (FORTRAN Code for Interpreting the Complex Chemical Kinetics and Transport Properties of a Premixed, Laminar, Steady-State Flame), U.S. Army Research Laboratory, developed 1990–2002, unpublished.

35. Anderson, R. J., J. F. Nuzman, W. R. Anderson, and J. J. Bitely. ChemPlot Computer Code (JAVA Code for Rapid, On-Line Visualization of Complex Chemical-Kinetic Code Outputs), U.S. Army Research Laboratory, developed 1997–2002, unpublished.

36. Anderson, R. J., and W. R. Anderson. ELEMAP Computer Code (JAVA Computer Code for Visualization of Chemical-Pathways Diagrams for Complex Chemical-Kinetic Code Outputs), U.S. Army Research Laboratory, developed 1999–2002, unpublished.

37. Miller, M. S. "Three-Phase Combustion Modelling: Frozen Ozone, a Prototype System." *Proceedings of the Materials Research Society Symposium: Decomposition, Combustion and Detonation Chemistry of Energetic Materials*, T. B. Brill, T. P. Russell, W. C. Tao, and R. B. Wardle (eds.), Materials Research Sociey, Pittsburgh, PA, pp. 169–180, 1996.

38. Zenin, A. A. "Structure of Temperature Distribution in Steady-State Burning of a Ballistite Powder." *Fizika Goreniya i Vzryva*, vol. 2, no. 3, pp. 67–76, 1966.

APPENDIX A: Ingredient Database

```
* INGREDIENT PROPERTY DATABASE:
INGRED   NC1                                                    !cellulose mononitrate
MOLWT    207.1396                                               ! g/mole
RHOS     1.520    0.  0.  0.  0.                                ! g/cc
CPS      -625.8  9.099  -0.04810  1.129E-4  -9.840E-8          ! cp(cal/g-K)*W/R
HREF     -1.99E5                                                ! cal/mole
TREF     298.15                                                 ! K
NPROD    6                                                      !
NO2      1.                                                     ! moles/mole
CH2O     2.                                                     ! moles/mole
HCO      1.                                                     ! moles/mole
CH2      1.                                                     ! moles/mole
CO       2.                                                     ! moles/mole
H        2.                                                     ! moles/mole
END
*
INGRED   NC2                                                    ! cellulose dinitrate
MOLWT    252.1372                                               ! g/mole
RHOS     1.578    0.  0.  0.  0.                                ! g/cc
CPS      -761.7  11.08  -0.05854  1.375E-4  -1.198E-7          ! cp(cal/g-K)*W/R
HREF     -1.73E5                                                ! cal/mole
TREF     298.15                                                 ! K
NPROD    6                                                      !
NO2      2.                                                     ! moles/mole
CH2O     2.                                                     ! moles/mole
HCO      1.                                                     ! moles/mole
CH2      1.                                                     ! moles/mole
CO       2.                                                     ! moles/mole
H        1.                                                     ! moles/mole
END
*
INGRED   NC3                                                    ! cellulose trinitrate
MOLWT    297.1348                                               ! g/mole
RHOS     1.664    0.  0.  0.  0.                                ! g/cc
CPS      -897.7  13.05  -0.06899  1.620E-4  -1.412E-7          ! cp(cal/g-K)*W/R
HREF     -1.45E5                                                ! cal/mole
TREF     298.15                                                 ! K
NPROD    5                                                      !
NO2      3.                                                     ! moles/mole
CH2O     2.                                                     ! moles/mole
HCO      1.                                                     ! moles/mole
CH2      1.                                                     ! moles/mole
CO       2.                                                     ! moles/mole
END
*
INGRED   NG                                                     ! nitroglycerine
MOLWT    227.0880                                               ! g/mole
RHOS     1.59    0.  0.  0.  0.                                 ! g/cc
CPS      34.0    0.  0.  0.  0.                                 ! cp(cal/g-K)*W/R
HREF     -89.6E3                                                ! cal/mole
TREF     298.15                                                 ! K
NPROD    5                                                      !
NO2      2.6                                                    ! moles/mole
HONO     0.4                                                    ! moles/mole
CH2O     2.                                                     ! moles/mole
HCO      0.6                                                    ! moles/mole
CO       0.4                                                    ! moles/mole
END
*


INGRED   DEGDN                                                  ! diethyleneglycol dinitrate
MOLWT    196.1176                                               ! g/mole
```

```
RHOS      1.38     0.   0.   0.   0.      ! g/cc
CPS       29.6     0.   0.   0.   0.      ! cp(cal/g-K)*W/R
HREF      -106.7E3                        ! cal/mole
TREF      298.15                          ! K
NPROD     9                               !
NO2       0.8333                          ! moles/mole
HONO      1.1667                          ! moles/mole
CHOCHO    0.50                            ! moles/mole
CH2O      1.3333                          ! moles/mole
HCO       0.50                            ! moles/mole
CH2       0.50                            ! moles/mole
CH3       0.3333                          ! moles/mole
CH4       0.1667                          ! moles/mole
CO        0.1667                          ! moles/mole
END
*
```

Key:

MOLWT: molecular weight of ingredient in g/mole

RHOS: density of ingredient in g/cm^3

CPS: Taylor series expansion coefficients of the quantity,
specific heat (cal/g-K) x molecular weight (g/mole) x universal gas constant (cal/mole-K)

HREF: heat of formation of the ingredient at the reference temperature TREF in K

NPROD: number of condensed-phase decomposition products

APPENDIX B: Gas-Phase Reaction Mechanism

```
CHEMKIN INTERPRETER OUTPUT: CHEMKIN-II Version 3.6 Apr. 1994
                            DOUBLE PRECISION

                          --------------------
                          ELEMENTS     ATOMIC
                          CONSIDERED   WEIGHT
                          --------------------
                           1. H        1.00797
                           2. C        12.0112
                           3. O        15.9994
                           4. N        14.0067
                          --------------------
```

SPECIES CONSIDERED	PHASE	CHARGE	MOLECULAR WEIGHT	TEMPERATURE LOW	TEMPERATURE HIGH	ELEMENT COUNT H	C	O	N	AR
1. CH2CO	G	0	42.03764	300.0	5000.0	2	2	1	0	0
2. CHOCHO	G	0	58.03704	300.0	5000.0	2	2	2	0	0
3. NO	G	0	30.00610	200.0	6000.0	0	0	1	1	0
4. N2	G	0	28.01340	300.0	5000.0	0	0	0	2	0
5. H	G	0	1.00797	300.0	5000.0	1	0	0	0	0
6. H2	G	0	2.01594	300.0	5000.0	2	0	0	0	0
7. H2O	G	0	18.01534	300.0	5000.0	2	0	1	0	0
8. CO	G	0	28.01055	300.0	5000.0	0	1	1	0	0
9. CO2	G	0	44.00995	300.0	5000.0	0	1	2	0	0
10. N2O	G	0	44.01280	300.0	5000.0	0	0	1	2	0
11. NH	G	0	15.01467	200.0	6000.0	1	0	0	1	0
12. HNO	G	0	31.01407	200.0	6000.0	1	0	1	1	0
13. HONO	G	0	47.01347	300.0	5000.0	1	0	2	1	0
14. NO2	G	0	46.00550	300.0	5000.0	0	0	2	1	0
15. OH	G	0	17.00737	300.0	5000.0	1	0	1	0	0
16. O	G	0	15.99940	300.0	5000.0	0	0	1	0	0
17. N	G	0	14.00670	300.0	5000.0	0	0	0	1	0
18. HNNO	G	0	45.02077	300.0	5000.0	1	0	1	2	0
19. NNH	G	0	29.02137	250.0	4000.0	1	0	0	2	0
20. CH2O	G	0	30.02649	200.0	3500.0	2	1	1	0	0
21. HCO	G	0	29.01852	200.0	6000.0	1	1	1	0	0
22. O2	G	0	31.99880	300.0	5000.0	0	0	2	0	0
23. HO2	G	0	33.00677	300.0	5000.0	1	0	2	0	0
24. H2O2	G	0	34.01474	300.0	5000.0	2	0	2	0	0
25. CH3	G	0	15.03506	300.0	5000.0	3	1	0	0	0
26. CH2	G	0	14.02709	250.0	4000.0	2	1	0	0	0
27. CH2(S)	G	0	14.02709	300.0	4000.0	2	1	0	0	0
28. CH4	G	0	16.04303	300.0	5000.0	4	1	0	0	0
29. CH2OH	G	0	31.03446	250.0	4000.0	3	1	1	0	0
30. CH3OH	G	0	32.04243	300.0	5000.0	4	1	1	0	0
31. HCCO	G	0	41.02967	300.0	4000.0	1	2	1	0	0
32. CH3O	G	0	31.03446	300.0	3000.0	3	1	1	0	0
33. CH	G	0	13.01912	300.0	5000.0	1	1	0	0	0
34. C	G	0	12.01115	300.0	5000.0	0	1	0	0	0
35. C2H6	G	0	30.07012	300.0	4000.0	6	2	0	0	0

36. C2H5	G	0	29.06215	300.0	5000.0	5	2	0	0	0
37. C2H4	G	0	28.05418	300.0	5000.0	4	2	0	0	0
38. C2H3	G	0	27.04621	300.0	5000.0	3	2	0	0	0
39. C2H2	G	0	26.03824	300.0	5000.0	2	2	0	0	0
40. C2H	G	0	25.03027	300.0	4000.0	1	2	0	0	0
41. HCCOH	G	0	42.03764	300.0	4000.0	2	2	1	0	0
42. NH3	G	0	17.03061	300.0	5000.0	3	0	0	1	0
43. NH2	G	0	16.02264	200.0	6000.0	2	0	0	1	0
44. HOCO	G	0	45.01792	300.0	4000.0	1	1	2	0	0
45. N2H2	G	0	30.02934	300.0	5000.0	2	0	0	2	0
46. N2H3	G	0	31.03731	300.0	5000.0	3	0	0	2	0
47. N2H4	G	0	32.04528	300.0	5000.0	4	0	0	2	0
48. NO3	G	0	62.00490	300.0	5000.0	0	0	3	1	0
49. HCN	G	0	27.02582	200.0	6000.0	1	1	0	1	0
50. HNCO	G	0	43.02522	200.0	6000.0	1	1	1	1	0
51. HOCN	G	0	43.02522	300.0	4000.0	1	1	1	1	0
52. HCNO	G	0	43.02522	250.0	4000.0	1	1	1	1	0
53. CN	G	0	26.01785	300.0	5000.0	0	1	0	1	0
54. H2CN	G	0	28.03379	300.0	4000.0	2	1	0	1	0
55. C2N2	G	0	52.03570	300.0	5000.0	0	2	0	2	0
56. HNC	G	0	27.02582	300.0	5000.0	1	1	0	1	0
57. NCNO	G	0	56.02395	300.0	4000.0	0	1	1	2	0
58. NCN	G	0	40.02455	300.0	4000.0	0	1	0	2	0
59. NCO	G	0	42.01725	200.0	6000.0	0	1	1	1	0

REACTIONS CONSIDERED	(k = A T**b exp(-E/RT)) A	b	E
1. NO2(+M)=NO+O(+M)	7.600E+18	-1.27	73290.0
Low pressure limit: 0.24700E+29 -0.33700E+01 0.74800E+05			
T&H VALUES 0.95000E+00 -0.10000E-03			
N2O Enhanced by 1.500E+00			
H2O Enhanced by 4.400E+00			
N2 Enhanced by 1.000E+00			
CO2 Enhanced by 2.300E+00			
2. N2O(+M)=N2+O(+M)	1.260E+12	0.00	62620.0
Low pressure limit: 0.59700E+15 0.00000E+00 0.56640E+05			
N2O Enhanced by 5.000E+00			
H2O Enhanced by 7.500E+00			
N2 Enhanced by 1.000E+00			
CO2 Enhanced by 3.200E+00			
O2 Enhanced by 8.200E-01			
3. H+NO(+M)=HNO(+M)	1.520E+15	-0.41	0.0
Low pressure limit: 0.89600E+20 -0.13200E+01 0.73500E+03			
T&H VALUE 0.82000E+00			
N2O Enhanced by 5.000E+00			
H2O Enhanced by 5.000E+00			
N2 Enhanced by 1.000E+00			
CO2 Enhanced by 1.300E+00			
4. NO+OH(+M)=HONO(+M)	1.988E+12	-0.05	-721.0
Low pressure limit: 0.50800E+24 -0.25100E+01 -0.67600E+02			
T&H VALUE 0.62000E+00			
N2O Enhanced by 5.000E+00			
H2O Enhanced by 8.300E+00			
N2 Enhanced by 1.000E+00			

```
      CO2                 Enhanced by    1.500E+00
 5. HCN(+M)=H+CN(+M)                                 8.300E+17   -0.93   123800.0
    Low pressure limit:  0.35700E+27 -0.26000E+01  0.12490E+06
    T&H VALUES  0.95000E+00 -0.10000E-03
      N2O                 Enhanced by    5.000E+00
      H2O                 Enhanced by    5.000E+00
      N2                  Enhanced by    1.000E+00
      CO2                 Enhanced by    1.600E+00
 6. CN+CN(+M)=C2N2(+M)                               5.660E+12    0.00        0.0
    Low pressure limit:  0.34300E+26 -0.26100E+01  0.00000E+00
    T&H VALUE  0.50000E+00
      N2O                 Enhanced by    5.000E+00
      H2O                 Enhanced by    5.000E+00
      N2                  Enhanced by    1.000E+00
      CO2                 Enhanced by    1.600E+00
 7. HNCO(+M)=NH+CO(+M)                               6.000E+13    0.00    99800.0
    Low pressure limit:  0.21700E+29 -0.31000E+01  0.10190E+06
    T&H VALUES  0.90000E+00 -0.20000E-03
      N2O                 Enhanced by    5.000E+00
      H2O                 Enhanced by    5.000E+00
      N2                  Enhanced by    1.000E+00
      CO2                 Enhanced by    1.600E+00
 8. HCN+H(+M)=H2CN(+M)                               3.310E+13    0.00     4844.0
    Low pressure limit:  0.16000E+25 -0.27300E+01  0.76600E+04
    T&H VALUES  0.95000E+00 -0.10000E-03
      N2O                 Enhanced by    5.000E+00
      H2O                 Enhanced by    5.000E+00
      N2                  Enhanced by    1.000E+00
      CO2                 Enhanced by    2.000E+00
 9. CN+NO(+M)=NCNO(+M)                               3.980E+13    0.00        0.0
    Low pressure limit:  0.15600E+37 -0.62000E+01  0.48780E+04
    T&H VALUE  0.65000E+00
      N2O                 Enhanced by    5.000E+00
      H2O                 Enhanced by    5.000E+00
      N2                  Enhanced by    1.000E+00
      CO2                 Enhanced by    2.000E+00
10. CN+M=C+N+M                                       2.500E+14    0.00   141100.0
      N2                  Enhanced by    1.500E+00
      CO2                 Enhanced by    2.400E+00
11. NO+M=N+O+M                                       1.400E+15    0.00   148430.0
      N2                  Enhanced by    1.000E+00
      H2                  Enhanced by    2.200E+00
      H2O                 Enhanced by    6.700E+00
      CO2                 Enhanced by    3.000E+00
      N2O                 Enhanced by    2.200E+00
12. N2+M=N+N+M                                       3.710E+21   -1.60   225000.0
13. N2O+N=N2+NO                                      1.000E+13    0.00    19870.0
14. NO2+N=N2O+O                                      5.010E+12    0.00        0.0
15. NO2+N=NO+NO                                      3.980E+12    0.00        0.0
16. NO2+NO2=NO+NO+O2                                 1.630E+12    0.00    26120.0
17. NO2+NO2=NO+NO3                                   9.640E+09    0.73    20920.0
18. NO2+NO3=NO+NO2+O2                                1.400E+11    0.00     3180.0
19. HNO+NO=N2O+OH                                    1.700E+13    0.00    29590.0
20. HNO+O2=HO2+NO                                    1.000E+13    0.00    25000.0
21. HNO+NO2=HONO+NO                                  6.000E+11    0.00     1987.0
22. HONO+O=OH+NO2                                    1.200E+13    0.00     5961.0
23. HONO+OH=H2O+NO2                                  1.270E+10    1.00      135.0
24. HNO+O=OH+NO                                      3.610E+13    0.00        0.0
```

25. NH+O=NO+H			5.500E+13	0.00	0.0
26. NH+O=N+OH			3.720E+13	0.00	0.0
27. NH+NH=N2+H+H			5.100E+13	0.00	0.0
28. NH+M=N+H+M			2.650E+14	0.00	75510.0
29. NH2+NO=N2O+H2			5.000E+13	0.00	24640.0
30. CH+O2=HCO+O			3.300E+13	0.00	0.0
31. CH+O=CO+H			5.700E+13	0.00	0.0
32. CH+OH=HCO+H			3.000E+13	0.00	0.0
33. CH+CO2=HCO+CO			3.400E+12	0.00	690.0
34. CH+H=C+H2			1.500E+14	0.00	0.0
35. C+O2=CO+O			2.000E+13	0.00	0.0
36. C+OH=CO+H			5.000E+13	0.00	0.0
37. HCO+OH=H2O+CO			1.000E+14	0.00	0.0
38. HCO+M=H+CO+M			2.500E+14	0.00	16802.0
CO	Enhanced by	1.900E+00			
H2	Enhanced by	1.900E+00			
CO2	Enhanced by	3.000E+00			
H2O	Enhanced by	5.000E+00			
39. HCO+H=CO+H2			1.190E+13	0.25	0.0
40. HCO+O=CO+OH			3.000E+13	0.00	0.0
41. HCO+O=CO2+H			3.000E+13	0.00	0.0
42. HCO+O2=HO2+CO			3.300E+13	-0.40	0.0
43. CO+O(+M)=CO2(+M)			1.800E+10	0.00	2380.0
Low pressure limit: 0.13500E+25 -0.27900E+01 0.41900E+04					
T&H VALUE 0.10000E+01					
H2O	Enhanced by	1.200E+01			
H2	Enhanced by	2.500E+00			
CO	Enhanced by	1.900E+00			
CO2	Enhanced by	3.800E+00			
N2O	Enhanced by	5.000E+00			
44. CO+OH=CO2+H			1.510E+07	1.30	-758.0
45. CO+O2=CO2+O			2.530E+12	0.00	47688.0
46. HO2+CO=CO2+OH			5.800E+13	0.00	22934.0
47. O+HCCO=H+2CO			1.000E+14	0.00	0.0
48. HCCO+O2=2CO+OH			1.600E+12	0.00	854.0
49. H2+O2=2OH			1.700E+13	0.00	47780.0
50. OH+H2=H2O+H			2.160E+08	1.50	3430.0
51. O2+H=O+OH			3.520E+16	-0.70	17070.0
52. O+H2=OH+H			5.060E+04	2.67	6290.0
53. H+O2+M=HO2+M			3.610E+17	-0.72	0.0
H2O	Enhanced by	1.860E+01			
CO2	Enhanced by	4.200E+00			
H2	Enhanced by	2.900E+00			
CO	Enhanced by	2.100E+00			
N2	Enhanced by	1.300E+00			
54. OH+HO2=H2O+O2			7.500E+12	0.00	0.0
55. H+HO2=2OH			1.690E+14	0.00	874.0
56. O+HO2=O2+OH			1.400E+13	0.00	1073.0
57. 2OH=O+H2O			6.000E+08	1.30	0.0
58. 2H+M=H2+M			1.000E+18	-1.00	0.0
H2	Enhanced by	0.000E+00			
H2O	Enhanced by	0.000E+00			
CO2	Enhanced by	0.000E+00			
59. 2H+H2=2H2			9.200E+16	-0.60	0.0
60. 2H+H2O=H2+H2O			6.000E+19	-1.25	0.0
61. 2H+CO2=H2+CO2			5.490E+20	-2.00	0.0
62. H+OH+M=H2O+M			1.600E+22	-2.00	0.0
H2O	Enhanced by	5.000E+00			

63.	H+O+M=OH+M		6.200E+16	-0.60	0.0
	H2O	Enhanced by	5.000E+00		
64.	O+O+M=O2+M		1.890E+13	0.00	-1788.0
65.	H+HO2=H2+O2		6.630E+13	0.00	2126.0
66.	2HO2=H2O2+O2		1.800E+12	0.00	0.0
67.	H2O2+M=2OH+M		1.300E+17	0.00	45500.0
68.	H2O2+H=HO2+H2		4.820E+13	0.00	7948.0
69.	H2O2+OH=H2O+HO2		1.750E+12	0.00	318.0
70.	CH+N2=HCN+N		3.000E+11	0.00	13600.0
71.	CN+N=C+N2		1.040E+15	-0.50	0.0
72.	C+NO=CN+O		6.600E+13	0.00	0.0
73.	HCCO+NO=HCNO+CO		2.000E+13	0.00	0.0
74.	HCNO+H=HCN+OH		1.000E+14	0.00	12000.0
75.	CH+N=CN+H		1.300E+13	0.00	0.0
76.	HCCO+N=HCN+CO		5.000E+13	0.00	0.0
77.	HCN+OH=CN+H2O		3.900E+06	1.83	10290.0
78.	OH+HCN=HOCN+H		5.850E+04	2.40	12500.0
79.	OH+HCN=HNCO+H		1.980E-03	4.00	1000.0
80.	OH+HCN=NH2+CO		7.830E-04	4.00	4000.0
81.	HOCN+H=HNCO+H		1.000E+13	0.00	0.0
82.	HCN+O=NCO+H		1.380E+04	2.64	4980.0
83.	HCN+O=NH+CO		3.450E+03	2.64	4980.0
84.	HCN+O=CN+OH		2.700E+09	1.58	26600.0
85.	CN+H2=HCN+H		3.610E+08	1.55	3000.0
86.	CN+O=CO+N		2.050E+13	0.00	417.0
87.	CN+O2=NCO+O		2.600E+14	-0.50	0.0
88.	CN+OH=NCO+H		4.000E+13	0.00	0.0
89.	CN+HCN=C2N2+H		1.510E+07	1.71	1530.0
90.	CN+NO2=NCO+NO		6.160E+15	-0.75	344.0
91.	CN+CO2=NCO+CO		3.670E+06	2.16	26900.0
92.	CN+N2O=NCN+NO		2.400E+13	0.00	13330.0
93.	C2N2+O=NCO+CN		4.570E+12	0.00	8880.0
94.	C2N2+OH=HOCN+CN		1.860E+11	0.00	2900.0
95.	NO+HO2=NO2+OH		2.110E+12	0.00	-479.0
96.	NO2+H=NO+OH		1.300E+14	0.00	361.0
97.	NO2+O=NO+O2		3.900E+12	0.00	-238.0
98.	NCO+H=NH+CO		5.400E+13	0.00	0.0
99.	NCO+O=NO+CO		4.520E+13	0.00	0.0
100.	NCO+N=N2+CO		2.000E+13	0.00	0.0
101.	NCO+OH=NO+CO+H		2.000E+13	0.00	7500.0
102.	NCO+M=N+CO+M		1.140E+23	-1.95	59930.0
	N2O	Enhanced by	5.000E+00		
	H2O	Enhanced by	5.000E+00		
	N2	Enhanced by	1.000E+00		
	CO2	Enhanced by	1.500E+00		
103.	NCO+NO=N2O+CO		8.800E+17	-1.78	790.0
104.	NCO+NO=CO2+N2		1.130E+18	-1.78	790.0
105.	NCO+H2=HNCO+H		2.070E+06	2.00	6020.0
106.	NCO+NO2=CO2+N2O		1.950E+13	-0.26	-620.0
107.	NCO+NO2=CO+NO+NO		1.770E+12	-0.26	-620.0
108.	NH+O2=HNO+O		4.610E+05	2.00	6500.0
109.	NH+O2=NO+OH		1.280E+06	1.50	100.0
110.	NH+NO=N2O+H		3.500E+14	-0.46	16.1
111.	NH+NO=N2+OH		2.160E+13	-0.23	0.0
112.	N2O+H=N2+OH		2.530E+10	0.00	4550.0
	Declared duplicate reaction...				
113.	N2O+H=N2+OH		2.230E+14	0.00	16750.0
	Declared duplicate reaction...				

114.	NNH+O=N2O+H			1.400E+14	-0.40	477.0
115.	NNH+O=NO+NH			3.300E+14	-0.23	-1013.0
116.	N2O+O=N2+O2			3.692E+12	0.00	15940.0
117.	N2O+O=NO+NO			9.155E+13	0.00	27680.0
118.	H+HNO=NH+OH			3.000E+14	0.00	18000.0
119.	NH+OH=N+H2O			5.000E+11	0.50	2000.0
120.	NH+N=N2+H			3.000E+13	0.00	0.0
121.	N+H2=NH+H			1.600E+14	0.00	25140.0
122.	HNO+H=NH2+O			3.500E+15	-0.30	28200.0
123.	NH2+O=NH+OH			6.750E+12	0.00	0.0
124.	NH2+OH=NH+H2O			4.000E+06	2.00	1000.0
125.	NH2+H=NH+H2			4.000E+13	0.00	3650.0
126.	NH2+NH=N2H2+H			1.500E+15	-0.50	0.0
127.	NH2+N=N2+H+H			7.200E+13	0.00	0.0
128.	NH2+O2=HNO+OH			4.500E+12	0.00	25000.0
129.	NH2+NH2=N2H2+H2			5.000E+11	0.00	0.0
130.	NH2+NH2=NH+NH3			5.000E+13	0.00	10000.0
131.	NH2+NH2=N2H3+H			1.790E+13	-0.35	11320.0
132.	NH2+NH2+M=N2H4+M			2.980E+47	-9.44	9680.0
133.	NH2+NO2=N2O+H2O			2.840E+18	-2.20	0.0
134.	NH+NO2=N2O+OH			1.000E+13	0.00	0.0
135.	N2H4+H=N2H3+H2			1.000E+12	0.50	2000.0
136.	N2H4+OH=N2H3+H2O			3.000E+10	0.68	1290.0
137.	N2H4+O=N2H3+OH			2.000E+13	0.00	1000.0
138.	N2H3=N2H2+H			1.200E+13	0.00	58000.0
139.	N2H3+H=N2H2+H2			1.000E+12	0.50	2000.0
140.	N2H3+OH=N2H2+H2O			3.000E+10	0.68	1290.0
141.	N2H3+O=N2H2+OH			2.000E+13	0.00	1000.0
142.	N2H2+M=NNH+H+M			5.000E+16	0.00	50000.0
	H2O	Enhanced by	1.500E+01			
	O2	Enhanced by	2.000E+00			
	N2	Enhanced by	2.000E+00			
	H2	Enhanced by	2.000E+00			
143.	N2H2+H=NNH+H2			5.000E+13	0.00	1000.0
144.	N2H2+O=NH2+NO			1.000E+13	0.00	0.0
145.	N2H2+O=NNH+OH			2.000E+13	0.00	1000.0
146.	N2H2+OH=NNH+H2O			1.000E+13	0.00	1000.0
147.	N2H2+NH=NNH+NH2			1.000E+13	0.00	1000.0
148.	N2H2+NH2=NH3+NNH			1.000E+13	0.00	1000.0
149.	NH2+NO=N2+H+OH			9.300E+11	0.00	0.0
150.	NH2+NO=N2+H2O			2.000E+20	-2.60	924.0
151.	NH3+OH=NH2+H2O			2.040E+06	2.04	566.0
152.	NH3+H=NH2+H2			5.420E+05	2.40	9917.0
153.	NH3+O=NH2+OH			9.400E+06	1.94	6460.0
154.	NH3+M=NH2+H+M			2.200E+16	0.00	93470.0
155.	NNH+NO=N2+HNO			2.000E+13	0.00	0.0
156.	NNH+H=N2+H2			1.000E+14	0.00	0.0
157.	NNH+OH=N2+H2O			5.000E+13	0.00	0.0
158.	NNH+NH2=N2+NH3			5.000E+13	0.00	0.0
159.	NNH+NH=N2+NH2			5.000E+13	0.00	0.0
160.	HNO+OH=NO+H2O			1.295E+07	1.88	-958.0
161.	H+HNO=H2+NO			4.460E+11	0.72	655.0
162.	HNO+NH2=NH3+NO			2.000E+13	0.00	1000.0
163.	N+NO=N2+O			3.270E+12	0.30	0.0
164.	O+NO=N+O2			3.800E+09	1.00	41375.0
165.	NO+H=N+OH			1.700E+14	0.00	48800.0
166.	HNO+HNO=N2O+H2O			3.630E-03	3.98	1190.0
167.	HNC+O=NH+CO			5.440E+12	0.00	0.0

168.	HNC+O=H+NCO	1.600E+01	3.08	-224.0
169.	HNC+OH=HNCO+H	2.800E+13	0.00	3696.0
170.	N2O+NO=N2+NO2	4.290E+13	0.00	47130.0
171.	NO+NO+NO=N2O+NO2	1.070E+10	0.00	26800.0
172.	HOCO+M=OH+CO+M	2.190E+23	-1.89	35270.0
173.	HNC+OH=CN+H2O	1.500E+12	0.00	7680.0
174.	HNC+NO2=HNCO+NO	1.000E+12	0.00	32000.0
175.	HNCO+O=CO2+NH	9.800E+07	1.41	8524.0
176.	HNCO+O=NCO+OH	2.200E+06	2.11	11430.0
177.	HNCO+O=HNO+CO	1.490E+08	1.57	44010.0
178.	HNCO+OH=H2O+NCO	4.790E+05	2.00	2560.0
179.	HNCO+OH=NH2+CO2	1.600E+05	2.00	2560.0
180.	HNCO+NH=NH2+NCO	2.000E+13	0.00	19300.0
181.	HNCO+H=NH2+CO	2.250E+07	1.70	3800.0
182.	CH+NO=HCN+O	1.100E+14	0.00	0.0
183.	CN+NO=NCO+N	5.500E+12	0.00	30620.0
184.	CN+NO=N2+CO	3.900E+11	0.00	27820.0
185.	CN+NO=NCN+O	1.800E+13	0.00	38190.0
186.	CO+NO2=NO+CO2	9.040E+13	0.00	33780.0
187.	CH+NO2=HCO+NO	1.010E+14	0.00	0.0
188.	H2+NO2=HONO+H	3.210E+12	0.00	28810.0
189.	NNH=N2+H	3.000E+08	0.00	0.0
	Declared duplicate reaction...			
190.	NNH+M=N2+H+M	1.000E+13	0.50	3060.0
	Declared duplicate reaction...			
191.	HCN+M=HNC+M	4.360E+26	-3.34	50194.0
192.	HNO+NO+NO=HNNO+NO2	1.700E+11	0.00	2100.0
193.	HNNO+NO=NNH+NO2	3.200E+12	0.00	270.0
194.	HNNO+NO=N2+HONO	2.600E+11	0.00	810.0
195.	HNNO+M=H+N2O+M	2.200E+15	0.00	21600.0
196.	HNNO+M=N2+OH+M	1.000E+15	0.00	25600.0
197.	HCO+NO=HNO+CO	7.230E+12	0.00	0.0
198.	O+CH2<=>H+HCO	8.000E+13	0.00	0.0
199.	O+CH2(S)<=>H2+CO	1.500E+13	0.00	0.0
200.	O+CH2(S)<=>H+HCO	1.500E+13	0.00	0.0
201.	O+CH3<=>H+CH2O	8.430E+13	0.00	0.0
202.	O+CH4<=>OH+CH3	1.020E+09	1.50	8600.0
203.	O+CH2O<=>OH+HCO	3.900E+13	0.00	3540.0
204.	O+CH2OH<=>OH+CH2O	1.000E+13	0.00	0.0
205.	O+CH3O<=>OH+CH2O	1.000E+13	0.00	0.0
206.	O+CH3OH<=>OH+CH2OH	3.880E+05	2.50	3100.0
207.	O+CH3OH<=>OH+CH3O	1.300E+05	2.50	5000.0
208.	O+C2H<=>CH+CO	5.000E+13	0.00	0.0
209.	O+C2H2<=>H+HCCO	1.020E+07	2.00	1900.0
210.	O+C2H2<=>OH+C2H	4.600E+19	-1.41	28950.0
211.	O+C2H2<=>CO+CH2	1.020E+07	2.00	1900.0
212.	O+C2H3<=>H+CH2CO	3.000E+13	0.00	0.0
213.	O+C2H4<=>CH3+HCO	1.920E+07	1.83	220.0
214.	O+C2H5<=>CH3+CH2O	1.320E+14	0.00	0.0
215.	O+C2H6<=>OH+C2H5	8.980E+07	1.92	5690.0
216.	O+CH2CO<=>OH+HCCO	1.000E+13	0.00	8000.0
217.	O+CH2CO<=>CH2+CO2	1.750E+12	0.00	1350.0
218.	O2+CH2O<=>HO2+HCO	1.000E+14	0.00	40000.0
219.	H+CH2(+M)<=>CH3(+M)	2.500E+16	-0.80	0.0
	Low pressure limit: 0.32000E+28 -0.31400E+01 0.12300E+04			
	TROE centering: 0.68000E+00 0.78000E+02 0.19950E+04 0.55900E+04			
	H2 Enhanced by 2.000E+00			
	H2O Enhanced by 6.000E+00			

```
      CH4                 Enhanced by    2.000E+00
      CO                  Enhanced by    1.500E+00
      CO2                 Enhanced by    2.000E+00
      C2H6                Enhanced by    3.000E+00
220. H+CH2(S)<=>CH+H2                                 3.000E+13    0.00         0.0
221. H+CH3(+M)<=>CH4(+M)                              1.270E+16   -0.63       383.0
     Low pressure limit:  0.24770E+34 -0.47600E+01  0.24400E+04
     TROE centering:      0.78300E+00  0.74000E+02  0.29410E+04  0.69640E+04
      H2                  Enhanced by    2.000E+00
      H2O                 Enhanced by    6.000E+00
      CH4                 Enhanced by    2.000E+00
      CO                  Enhanced by    1.500E+00
      CO2                 Enhanced by    2.000E+00
      C2H6                Enhanced by    3.000E+00
222. H+CH4<=>CH3+H2                                   6.600E+08    1.62     10840.0
223. H+HCO(+M)<=>CH2O(+M)                             1.090E+12    0.48      -260.0
     Low pressure limit:  0.13500E+25 -0.25700E+01  0.14250E+04
     TROE centering:      0.78240E+00  0.27100E+03  0.27550E+04  0.65700E+04
      H2                  Enhanced by    2.000E+00
      H2O                 Enhanced by    6.000E+00
      CH4                 Enhanced by    2.000E+00
      CO                  Enhanced by    1.500E+00
      CO2                 Enhanced by    2.000E+00
      C2H6                Enhanced by    3.000E+00
224. H+CH2O(+M)<=>CH2OH(+M)                           5.400E+11    0.45      3600.0
     Low pressure limit:  0.12700E+33 -0.48200E+01  0.65300E+04
     TROE centering:      0.71870E+00  0.10300E+03  0.12910E+04  0.41600E+04
      H2                  Enhanced by    2.000E+00
      H2O                 Enhanced by    6.000E+00
      CH4                 Enhanced by    2.000E+00
      CO                  Enhanced by    1.500E+00
      CO2                 Enhanced by    2.000E+00
      C2H6                Enhanced by    3.000E+00
225. H+CH2O(+M)<=>CH3O(+M)                            5.400E+11    0.45      2600.0
     Low pressure limit:  0.22000E+31 -0.48000E+01  0.55600E+04
     TROE centering:      0.75800E+00  0.94000E+02  0.15550E+04  0.42000E+04
      H2                  Enhanced by    2.000E+00
      H2O                 Enhanced by    6.000E+00
      CH4                 Enhanced by    2.000E+00
      CO                  Enhanced by    1.500E+00
      CO2                 Enhanced by    2.000E+00
      C2H6                Enhanced by    3.000E+00
226. H+CH2O<=>HCO+H2                                  2.300E+10    1.05      3275.0
227. H+CH2OH(+M)<=>CH3OH(+M)                          1.800E+13    0.00         0.0
     Low pressure limit:  0.30000E+32 -0.48000E+01  0.33000E+04
     TROE centering:      0.76790E+00  0.33800E+03  0.18120E+04  0.50810E+04
      H2                  Enhanced by    2.000E+00
      H2O                 Enhanced by    6.000E+00
      CH4                 Enhanced by    2.000E+00
      CO                  Enhanced by    1.500E+00
      CO2                 Enhanced by    2.000E+00
      C2H6                Enhanced by    3.000E+00
228. H+CH2OH<=>H2+CH2O                                2.000E+13    0.00         0.0
229. H+CH2OH<=>OH+CH3                                 1.200E+13    0.00         0.0
230. H+CH2OH<=>CH2(S)+H2O                             6.000E+12    0.00         0.0
231. H+CH3O(+M)<=>CH3OH(+M)                           5.000E+13    0.00         0.0
     Low pressure limit:  0.86000E+29 -0.40000E+01  0.30250E+04
     TROE centering:      0.89020E+00  0.14400E+03  0.28380E+04  0.45569E+05
```

```
        H2                  Enhanced by    2.000E+00
        H2O                 Enhanced by    6.000E+00
        CH4                 Enhanced by    2.000E+00
        CO                  Enhanced by    1.500E+00
        CO2                 Enhanced by    2.000E+00
        C2H6                Enhanced by    3.000E+00
232. H+CH3O<=>H+CH2OH                          3.400E+06    1.60         0.0
233. H+CH3O<=>H2+CH2O                          2.000E+13    0.00         0.0
234. H+CH3O<=>OH+CH3                           3.200E+13    0.00         0.0
235. H+CH3O<=>CH2(S)+H2O                       1.600E+13    0.00         0.0
236. H+CH3OH<=>CH2OH+H2                        1.700E+07    2.10      4870.0
237. H+CH3OH<=>CH3O+H2                         4.200E+06    2.10      4870.0
238. H+C2H(+M)<=>C2H2(+M)                      1.000E+17   -1.00         0.0
     Low pressure limit:  0.37500E+34 -0.48000E+01  0.19000E+04
     TROE centering:      0.64640E+00  0.13200E+03  0.13150E+04  0.55660E+04
        H2                  Enhanced by    2.000E+00
        H2O                 Enhanced by    6.000E+00
        CH4                 Enhanced by    2.000E+00
        CO                  Enhanced by    1.500E+00
        CO2                 Enhanced by    2.000E+00
        C2H6                Enhanced by    3.000E+00
239. H+C2H2(+M)<=>C2H3(+M)                     5.600E+12    0.00      2400.0
     Low pressure limit:  0.38000E+41 -0.72700E+01  0.72200E+04
     TROE centering:      0.75070E+00  0.98500E+02  0.13020E+04  0.41670E+04
        H2                  Enhanced by    2.000E+00
        H2O                 Enhanced by    6.000E+00
        CH4                 Enhanced by    2.000E+00
        CO                  Enhanced by    1.500E+00
        CO2                 Enhanced by    2.000E+00
        C2H6                Enhanced by    3.000E+00
240. H+C2H3(+M)<=>C2H4(+M)                     6.080E+12    0.27       280.0
     Low pressure limit:  0.14000E+31 -0.38600E+01  0.33200E+04
     TROE centering:      0.78200E+00  0.20750E+03  0.26630E+04  0.60950E+04
        H2                  Enhanced by    2.000E+00
        H2O                 Enhanced by    6.000E+00
        CH4                 Enhanced by    2.000E+00
        CO                  Enhanced by    1.500E+00
        CO2                 Enhanced by    2.000E+00
        C2H6                Enhanced by    3.000E+00
241. H+C2H3<=>H2+C2H2                          3.000E+13    0.00         0.0
242. H+C2H4(+M)<=>C2H5(+M)                     1.080E+12    0.45      1820.0
     Low pressure limit:  0.12000E+43 -0.76200E+01  0.69700E+04
     TROE centering:      0.97530E+00  0.21000E+03  0.98400E+03  0.43740E+04
        H2                  Enhanced by    2.000E+00
        H2O                 Enhanced by    6.000E+00
        CH4                 Enhanced by    2.000E+00
        CO                  Enhanced by    1.500E+00
        CO2                 Enhanced by    2.000E+00
        C2H6                Enhanced by    3.000E+00
243. H+C2H4<=>C2H3+H2                          1.325E+06    2.53     12240.0
244. H+C2H5(+M)<=>C2H6(+M)                     5.210E+17   -0.99      1580.0
     Low pressure limit:  0.19900E+42 -0.70800E+01  0.66850E+04
     TROE centering:      0.84220E+00  0.12500E+03  0.22190E+04  0.68820E+04
        H2                  Enhanced by    2.000E+00
        H2O                 Enhanced by    6.000E+00
        CH4                 Enhanced by    2.000E+00
        CO                  Enhanced by    1.500E+00
        CO2                 Enhanced by    2.000E+00
```

```
      C2H6                Enhanced by    3.000E+00
245. H+C2H5<=>H2+C2H4                              2.000E+12    0.00        0.0
246. H+C2H6<=>C2H5+H2                              1.150E+08    1.90     7530.0
247. H+HCCO<=>CH2(S)+CO                            1.000E+14    0.00        0.0
248. H+HCCOH<=>H+CH2CO                             1.000E+13    0.00        0.0
249. H2+CO(+M)<=>CH2O(+M)                          4.300E+07    1.50    79600.0
     Low pressure limit:  0.50700E+28 -0.34200E+01  0.84350E+05
     TROE centering:      0.93200E+00  0.19700E+03  0.15400E+04  0.10300E+05
        H2                Enhanced by    2.000E+00
        H2O               Enhanced by    6.000E+00
        CH4               Enhanced by    2.000E+00
        CO                Enhanced by    1.500E+00
        CO2               Enhanced by    2.000E+00
        C2H6              Enhanced by    3.000E+00
250. 2OH(+M)<=>H2O2(+M)                            7.400E+13   -0.37        0.0
     Low pressure limit:  0.23000E+19 -0.90000E+00 -0.17000E+04
     TROE centering:      0.73460E+00  0.94000E+02  0.17560E+04  0.51820E+04
        H2                Enhanced by    2.000E+00
        H2O               Enhanced by    6.000E+00
        CH4               Enhanced by    2.000E+00
        CO                Enhanced by    1.500E+00
        CO2               Enhanced by    2.000E+00
        C2H6              Enhanced by    3.000E+00
251. OH+CH2<=>H+CH2O                               2.000E+13    0.00        0.0
252. OH+CH2<=>CH+H2O                               1.130E+07    2.00     3000.0
253. OH+CH2(S)<=>H+CH2O                            3.000E+13    0.00        0.0
254. OH+CH3(+M)<=>CH3OH(+M)                        6.300E+13    0.00        0.0
     Low pressure limit:  0.27000E+39 -0.63000E+01  0.31000E+04
     TROE centering:      0.21050E+00  0.83500E+02  0.53980E+04  0.83700E+04
        H2                Enhanced by    2.000E+00
        H2O               Enhanced by    6.000E+00
        CH4               Enhanced by    2.000E+00
        CO                Enhanced by    1.500E+00
        CO2               Enhanced by    2.000E+00
        C2H6              Enhanced by    3.000E+00
255. OH+CH3<=>CH2+H2O                              5.600E+07    1.60     5420.0
256. OH+CH3<=>CH2(S)+H2O                           2.501E+13    0.00        0.0
257. OH+CH4<=>CH3+H2O                              1.000E+08    1.60     3120.0
258. OH+CH2O<=>HCO+H2O                             3.430E+09    1.18     -447.0
259. OH+CH2OH<=>H2O+CH2O                           5.000E+12    0.00        0.0
260. OH+CH3O<=>H2O+CH2O                            5.000E+12    0.00        0.0
261. OH+CH3OH<=>CH2OH+H2O                          1.440E+06    2.00     -840.0
262. OH+CH3OH<=>CH3O+H2O                           6.300E+06    2.00     1500.0
263. OH+C2H<=>H+HCCO                               2.000E+13    0.00        0.0
264. OH+C2H2<=>H+CH2CO                             2.180E-04    4.50    -1000.0
265. OH+C2H2<=>H+HCCOH                             5.040E+05    2.30    13500.0
266. OH+C2H2<=>C2H+H2O                             3.370E+07    2.00    14000.0
267. OH+C2H2<=>CH3+CO                              4.830E-04    4.00    -2000.0
268. OH+C2H3<=>H2O+C2H2                            5.000E+12    0.00        0.0
269. OH+C2H4<=>C2H3+H2O                            3.600E+06    2.00     2500.0
270. OH+C2H6<=>C2H5+H2O                            3.540E+06    2.12      870.0
271. OH+CH2CO<=>HCCO+H2O                           7.500E+12    0.00     2000.0
272. HO2+CH2<=>OH+CH2O                             2.000E+13    0.00        0.0
273. HO2+CH3<=>O2+CH4                              1.000E+12    0.00        0.0
274. HO2+CH3<=>OH+CH3O                             2.000E+13    0.00        0.0
275. HO2+CH2O<=>HCO+H2O2                           1.000E+12    0.00     8000.0
276. C+CH2<=>H+C2H                                 5.000E+13    0.00        0.0
277. C+CH3<=>H+C2H2                                5.000E+13    0.00        0.0
```

```
278. CH+H2<=>H+CH2                                    1.107E+08    1.79     1670.0
279. CH+H2O<=>H+CH2O                                  1.713E+13    0.00     -755.0
280. CH+CH2<=>H+C2H2                                  4.000E+13    0.00        0.0
281. CH+CH3<=>H+C2H3                                  3.000E+13    0.00        0.0
282. CH+CH4<=>H+C2H4                                  6.000E+13    0.00        0.0
283. CH+CO(+M)<=>HCCO(+M)                             5.000E+13    0.00        0.0
     Low pressure limit:  0.26900E+29 -0.37400E+01  0.19360E+04
     TROE centering:      0.57570E+00  0.23700E+03  0.16520E+04  0.50690E+04
        H2                Enhanced by    2.000E+00
        H2O               Enhanced by    6.000E+00
        CH4               Enhanced by    2.000E+00
        CO                Enhanced by    1.500E+00
        CO2               Enhanced by    2.000E+00
        C2H6              Enhanced by    3.000E+00
284. CH+CH2O<=>H+CH2CO                                9.460E+13    0.00     -515.0
285. CH+HCCO<=>CO+C2H2                                5.000E+13    0.00        0.0
286. CH2+O2<=>OH+HCO                                  1.320E+13    0.00     1500.0
287. CH2+H2<=>H+CH3                                   5.000E+05    2.00     7230.0
288. 2CH2<=>H2+C2H2                                   3.200E+13    0.00        0.0
289. CH2+CH3<=>H+C2H4                                 4.000E+13    0.00        0.0
290. CH2+CH4<=>2CH3                                   2.460E+06    2.00     8270.0
291. CH2+HCCO<=>C2H3+CO                               3.000E+13    0.00        0.0
292. CH2(S)+N2<=>CH2+N2                               1.500E+13    0.00      600.0
293. CH2(S)+O2<=>H+OH+CO                              2.800E+13    0.00        0.0
294. CH2(S)+O2<=>CO+H2O                               1.200E+13    0.00        0.0
295. CH2(S)+H2<=>CH3+H                                7.000E+13    0.00        0.0
296. CH2(S)+H2O(+M)<=>CH3OH(+M)                       2.000E+13    0.00        0.0
     Low pressure limit:  0.27000E+39 -0.63000E+01  0.31000E+04
     TROE centering:      0.15070E+00  0.13400E+03  0.23830E+04  0.72650E+04
        H2                Enhanced by    2.000E+00
        H2O               Enhanced by    6.000E+00
        CH4               Enhanced by    2.000E+00
        CO                Enhanced by    1.500E+00
        CO2               Enhanced by    2.000E+00
        C2H6              Enhanced by    3.000E+00
297. CH2(S)+H2O<=>CH2+H2O                             3.000E+13    0.00        0.0
298. CH2(S)+CH3<=>H+C2H4                              1.200E+13    0.00     -570.0
299. CH2(S)+CH4<=>2CH3                                1.600E+13    0.00     -570.0
300. CH2(S)+CO<=>CH2+CO                               9.000E+12    0.00        0.0
301. CH2(S)+CO2<=>CH2+CO2                             7.000E+12    0.00        0.0
302. CH2(S)+CO2<=>CO+CH2O                             1.400E+13    0.00        0.0
303. CH2(S)+C2H6<=>CH3+C2H5                           4.000E+13    0.00     -550.0
304. CH3+O2<=>O+CH3O                                  2.675E+13    0.00    28800.0
305. CH3+O2<=>OH+CH2O                                 3.600E+10    0.00     8940.0
306. CH3+H2O2<=>HO2+CH4                               2.450E+04    2.47     5180.0
307. 2CH3(+M)<=>C2H6(+M)                              2.120E+16   -0.97      620.0
     Low pressure limit:  0.17700E+51 -0.96700E+01  0.62200E+04
     TROE centering:      0.53250E+00  0.15100E+03  0.10380E+04  0.49700E+04
        H2                Enhanced by    2.000E+00
        H2O               Enhanced by    6.000E+00
        CH4               Enhanced by    2.000E+00
        CO                Enhanced by    1.500E+00
        CO2               Enhanced by    2.000E+00
        C2H6              Enhanced by    3.000E+00
308. 2CH3<=>H+C2H5                                    4.990E+12    0.10    10600.0
309. CH3+HCO<=>CH4+CO                                 2.648E+13    0.00        0.0
310. CH3+CH2O<=>HCO+CH4                               3.320E+03    2.81     5860.0
311. CH3+CH3OH<=>CH2OH+CH4                            3.000E+07    1.50     9940.0
```

```
312. CH3+CH3OH<=>CH3O+CH4                          1.000E+07    1.50      9940.0
313. CH3+C2H4<=>C2H3+CH4                           2.270E+05    2.00      9200.0
314. CH3+C2H6<=>C2H5+CH4                           6.140E+06    1.74     10450.0
315. CH2OH+O2<=>HO2+CH2O                           1.800E+13    0.00       900.0
316. CH3O+O2<=>HO2+CH2O                            4.280E-13    7.60     -3530.0
317. C2H+O2<=>HCO+CO                               5.000E+13    0.00      1500.0
318. C2H+H2<=>H+C2H2                               4.070E+05    2.40       200.0
319. C2H3+O2<=>HCO+CH2O                            3.980E+12    0.00      -240.0
320. C2H4(+M)<=>H2+C2H2(+M)                        8.000E+12    0.44     88770.0
     Low pressure limit:  0.70000E+51 -0.93100E+01  0.99860E+05
     TROE centering:      0.73450E+00  0.18000E+03  0.10350E+04  0.54170E+04
        H2                Enhanced by    2.000E+00
        H2O               Enhanced by    6.000E+00
        CH4               Enhanced by    2.000E+00
        CO                Enhanced by    1.500E+00
        CO2               Enhanced by    2.000E+00
        C2H6              Enhanced by    3.000E+00
321. C2H5+O2<=>HO2+C2H4                            8.400E+11    0.00      3875.0
322. 2HCCO<=>2CO+C2H2                              1.000E+13    0.00         0.0
323. NNH+CH3<=>CH4+N2                              2.500E+13    0.00         0.0
324. NNH+O2<=>HO2+N2                               5.000E+12    0.00         0.0
325. NNH+O<=>OH+N2                                 2.500E+13    0.00         0.0
326. NCO+O2<=>NO+CO2                               2.000E+12    0.00     20000.0
327. H2CN+N<=>N2+CH2                               6.000E+13    0.00       400.0
328. CH2+N2<=>HCN+NH                               1.000E+13    0.00     74000.0
329. CH2(S)+N2<=>NH+HCN                            1.000E+11    0.00     65000.0
330. C+NO<=>CO+N                                   2.900E+13    0.00         0.0
331. CH+NO<=>H+NCO                                 2.000E+13    0.00         0.0
332. CH+NO<=>N+HCO                                 3.000E+13    0.00         0.0
333. CH2+NO<=>H+HNCO                               3.100E+17   -1.38      1270.0
334. CH2+NO<=>OH+HCN                               2.900E+14   -0.69       760.0
335. CH2+NO<=>H+HCNO                               3.800E+13   -0.36       580.0
336. CH2(S)+NO<=>H+HNCO                            3.100E+17   -1.38      1270.0
337. CH2(S)+NO<=>OH+HCN                            2.900E+14   -0.69       760.0
338. CH2(S)+NO<=>H+HCNO                            3.800E+13   -0.36       580.0
339. CH3+NO<=>HCN+H2O                              9.600E+13    0.00     28800.0
340. CH3+NO<=>H2CN+OH                              1.000E+12    0.00     21750.0
341. HCNO+H<=>H+HNCO                               2.100E+15   -0.69      2850.0
342. HCNO+H<=>NH2+CO                               1.700E+14   -0.75      2890.0
343. CH3+N<=>H2CN+H                                6.100E+14   -0.31       290.0
344. CH3+N<=>HCN+H2                                3.700E+12    0.15       -90.0
345. HCO+HNO=CH2O+NO                               6.000E+11    0.00      2000.0
346. CH2O+NO2=HCO+HONO                             8.020E+02    2.77     13730.0
347. HCO+NO2=CO+HONO                               1.240E+23   -3.29      2355.0
348. HCO+NO2=H+CO2+NO                              8.390E+15   -0.75      1930.0
349. CHOCHO(+M)=HCO+HCO(+M)                        2.940E+14    0.00     67900.0
     Low pressure limit:  0.91900E+50 -0.94300E+01  0.74016E+05
        H2O               Enhanced by    1.200E+01
        N2                Enhanced by    1.500E+00
        NO                Enhanced by    1.500E+00
        CO2               Enhanced by    5.000E+00
        CH2O              Enhanced by    2.000E+00
        NO2               Enhanced by    5.000E+00
        CO                Enhanced by    5.000E+00
        CHOCHO            Enhanced by    5.000E+00
        H2                Enhanced by    1.500E+00
350. CHOCHO+OH=H2O+CO+HCO                          3.400E+09    1.18       447.0
351. CHOCHO+H=H2+CO+HCO                            4.580E+10    1.05      3280.0
```

352.	CHOCHO+O=OH+CO+HCO		4.130E+11	0.57	2762.0
353.	CHOCHO+NO2=HONO+CO+HCO		7.940E+11	0.00	19800.0
354.	CHOCHO+NO=HNO+HCO+CO		1.000E+13	0.00	41000.0
355.	HCO+HCO=CH2O+CO		3.000E+13	0.00	0.0
356.	HCO+HCO=H2+CO+CO		5.200E+12	0.00	0.0
357.	HCO+CHOCHO=CH2O+CO+HCO		1.000E+13	0.00	11000.0
358.	CH2CO(+M)=CH2+CO(+M)		3.000E+14	0.00	71000.0
	Low pressure limit:	0.36000E+16 0.00000E+00 0.59300E+05			
	H2O	Enhanced by 1.200E+01			
	N2	Enhanced by 1.500E+00			
	NO	Enhanced by 1.500E+00			
	CO2	Enhanced by 5.000E+00			
	CH2O	Enhanced by 2.000E+00			
	NO2	Enhanced by 5.000E+00			
	CO	Enhanced by 5.000E+00			
	CHOCHO	Enhanced by 5.000E+00			
	H2	Enhanced by 1.500E+00			
359.	CH2CO+O=CH2O+CO		7.630E+11	0.00	1351.0
360.	CH2CO+O=HCO+H+CO		7.630E+11	0.00	1351.0
361.	CH2CO+O=HCO+HCO		7.630E+11	0.00	1351.0
362.	CH2CO+OH=CH2O+HCO		3.330E+12	0.00	0.0
363.	CH2CO+OH=CH2OH+CO		3.330E+12	0.00	0.0
364.	CH2CO+OH=CH3+CO2		3.330E+12	0.00	0.0
365.	CH2CO+H=CH3+CO		1.800E+13	0.00	3380.0

NOTE: A units mole-cm-sec-K, E units cal/mole

APPENDIX C: Ranked Sensitivity Coefficients for Temperature at First Gas-Phase Grid Point for M10

M10 at 0.3 MPa

	REACTION	SENS COEFF	RELATIVE
348	HCO+NO2=H+CO2+NO	2.78803E-05	100.
347	HCO+NO2=CO+HONO	-1.32854E-05	47.7
197	HCO+NO=HNO+CO	-1.17427E-05	42.1
358	CH2CO(+M)=CH2+CO(+M)	-8.41978E-06	30.2
333	CH2+NO<=>H+HNCO	7.37790E-06	26.5
258	OH+CH2O<=>HCO+H2O	6.65532E-06	23.9
363	CH2CO+OH=CH2OH+CO	-3.79628E-06	13.6
96	NO2+H=NO+OH	3.15586E-06	11.3
23	HONO+OH=H2O+NO2	-2.39296E-06	8.58
364	CH2CO+OH=CH3+CO2	1.85426E-06	6.65
161	H+HNO=H2+NO	-1.37163E-06	4.92
4	NO+OH(+M)=HONO(+M)	-1.25716E-06	4.51
355	HCO+HCO=CH2O+CO	-8.12371E-07	2.91
37	HCO+OH=H2O+CO	-6.37046E-07	2.28
334	CH2+NO<=>OH+HCN	6.34423E-07	2.28
21	HNO+NO2=HONO+NO	4.83349E-07	1.73
3	H+NO(+M)=HNO(+M)	-3.74569E-07	1.34
39	HCO+H=CO+H2	-3.52485E-07	1.26
307	2CH3(+M)<=>C2H6(+M)	3.14182E-07	1.13
44	CO+OH=CO2+H	3.06234E-07	1.10

M10 at 1 MPa

	REACTION	SENS COEFF	RELATIVE
348	HCO+NO2=H+CO2+NO	2.60342E-05	100.
358	CH2CO(+M)=CH2+CO(+M)	-1.28926E-05	49.5
197	HCO+NO=HNO+CO	-1.24956E-05	48.0
333	CH2+NO<=>H+HNCO	1.15948E-05	44.5
347	HCO+NO2=CO+HONO	-1.04940E-05	40.3
258	OH+CH2O<=>HCO+H2O	5.22733E-06	20.1
96	NO2+H=NO+OH	4.00231E-06	15.4
363	CH2CO+OH=CH2OH+CO	-2.93146E-06	11.3
364	CH2CO+OH=CH3+CO2	1.75596E-06	6.74
161	H+HNO=H2+NO	-1.46945E-06	5.64
4	NO+OH(+M)=HONO(+M)	-1.38164E-06	5.31
23	HONO+OH=H2O+NO2	-1.19076E-06	4.57
334	CH2+NO<=>OH+HCN	1.04268E-06	4.01
3	H+NO(+M)=HNO(+M)	-8.95455E-07	3.44
355	HCO+HCO=CH2O+CO	-8.19318E-07	3.15
37	HCO+OH=H2O+CO	-6.37958E-07	2.45
226	H+CH2O<=>HCO+H2	-4.37761E-07	1.68
224	H+CH2O(+M)<=>CH2OH(M)	-4.06637E-07	1.56
39	HCO+H=CO+H2	-3.93122E-07	1.51
21	HNO+NO2=HONO+NO	3.82936E-07	1.47

M10 at 3 MPa

	REACTION	SENS COEFF	RELATIVE
348	HCO+NO2=H+CO2+NO	2.43126E-05	100.
358	CH2CO(+M)=CH2+CO(+M)	-1.50945E-05	62.1
333	CH2+NO<=>H+HNCO	1.39549E-05	57.4
197	HCO+NO=HNO+CO	-1.29137E-05	53.1
347	HCO+NO2=CO+HONO	-8.87004E-06	36.5
96	NO2+H=NO+OH	4.59229E-06	18.9
258	OH+CH2O<=>HCO+H2O	4.13161E-06	17.0
363	CH2CO+OH=CH2OH+CO	-2.36522E-06	9.73
3	H+NO(+M)=HNO(+M)	-1.92322E-06	7.91
364	CH2CO+OH=CH3+CO2	1.69719E-06	6.98
4	NO+OH(+M)=HONO(+M)	-1.38886E-06	5.71
334	CH2+NO<=>OH+HCN	1.32443E-06	5.45
161	H+HNO=H2+NO	-1.25639E-06	5.17
355	HCO+HCO=CH2O+CO	-6.68854E-07	2.75
23	HONO+OH=H2O+NO2	-5.58107E-07	2.30
224	H+CH2O(+M)<=>CH2OH(M)	-5.17345E-07	2.13
226	H+CH2O<=>HCO+H2	-4.93804E-07	2.03
37	HCO+OH=H2O+CO	-4.74586E-07	1.95
39	HCO+H=CO+H2	-3.20408E-07	1.32
362	CH2CO+OH=CH2O+HCO	-3.10802E-07	1.28

M10 at 10 MPa

	REACTION	SENS COEFF	RELATIVE
348	HCO+NO2=H+CO2+NO	7.63297E-06	100.
358	CH2CO(+M)=CH2+CO(+M)	-5.48671E-06	71.9
333	CH2+NO<=>H+HNCO	5.08409E-06	66.6
197	HCO+NO=HNO+CO	-4.47309E-06	58.6
347	HCO+NO2=CO+HONO	-2.74887E-06	36.0
96	NO2+H=NO+OH	1.74709E-06	22.9
3	H+NO(+M)=HNO(+M)	-1.40165E-06	18.4
258	OH+CH2O<=>HCO+H2O	9.52004E-07	12.5
363	CH2CO+OH=CH2OH+CO	-6.62082E-07	8.67
364	CH2CO+OH=CH3+CO2	6.02135E-07	7.89
334	CH2+NO<=>OH+HCN	5.15629E-07	6.76
4	NO+OH(+M)=HONO(+M)	-3.92474E-07	5.14
21	HNO+NO2=HONO+NO	-2.30541E-07	3.02
161	H+HNO=H2+NO	-1.98041E-07	2.59
224	H+CH2O(+M)<=>CH2OH(M)	-1.76869E-07	2.32
362	CH2CO+OH=CH2O+HCO	-1.62042E-07	2.12
346	CH2O+NO2=HCO+HONO	1.59035E-07	2.08
226	H+CH2O<=>HCO+H2	-1.20834E-07	1.58
355	HCO+HCO=CH2O+CO	-1.10547E-07	1.45
229	H+CH2OH<=>OH+CH3	1.09625E-07	1.44

M10 at 30 MPa

	REACTION	SENS COEFF	RELATIVE
348	HCO+NO2=H+CO2+NO	5.40707E-06	100.
358	CH2CO(+M)=CH2+CO(+M)	-5.39779E-06	99.8
333	CH2+NO<=>H+HNCO	5.17824E-06	95.8
197	HCO+NO=HNO+CO	-3.52571E-06	65.2
347	HCO+NO2=CO+HONO	-1.60825E-06	29.7
3	H+NO(+M)=HNO(+M)	-1.11895E-06	20.7
364	CH2CO+OH=CH3+CO2	1.00814E-06	18.6
258	OH+CH2O<=>HCO+H2O	9.89347E-07	18.3
96	NO2+H=NO+OH	9.88727E-07	18.3
4	NO+OH(+M)=HONO(+M)	9.05500E-07	16.7
23	HONO+OH=H2O+NO2	-7.66861E-07	14.2
161	H+HNO=H2+NO	-6.00413E-07	11.1
334	CH2+NO<=>OH+HCN	5.55476E-07	10.3
166	HNO+HNO=N2O+H2O	4.26282E-07	7.88
19	HNO+NO=N2O+OH	3.98435E-07	7.37
21	HNO+NO2=HONO+NO	-3.23451E-07	5.98
363	CH2CO+OH=CH2OH+CO	-3.11463E-07	5.76
160	HNO+OH=NO+H2O	-2.93799E-07	5.43
346	CH2O+NO2=HCO+HONO	2.93520E-07	5.43
335	CH2+NO<=>H+HCNO	-2.90532E-07	5.37
365	CH2CO+H=CH3+CO	2.73825E-07	5.06

M10 at 100 MPa

	REACTION	SENS COEFF	RELATIVE
333	CH2+NO<=>H+HNCO	4.79755E-06	100.
358	CH2CO(+M)=CH2+CO(+M)	-4.71752E-06	98.3
348	HCO+NO2=H+CO2+NO	3.90935E-06	81.5
197	HCO+NO=HNO+CO	-2.64954E-06	55.2
161	H+HNO=H2+NO	-1.32964E-06	27.7
4	NO+OH(+M)=HONO(+M)	1.08776E-06	22.7
19	HNO+NO=N2O+OH	1.07451E-06	22.4
23	HONO+OH=H2O+NO2	-1.03875E-06	21.7
364	CH2CO+OH=CH3+CO2	9.49475E-07	19.8
258	OH+CH2O<=>HCO+H2O	9.22588E-07	19.2
21	HNO+NO2=HONO+NO	-7.44033E-07	15.5
347	HCO+NO2=CO+HONO	-6.53324E-07	13.6
192	HNO+NO+NO=HNNO+NO2	5.99762E-07	12.5
3	H+NO(+M)=HNO(+M)	-5.96385E-07	12.4
166	HNO+HNO=N2O+H2O	5.53765E-07	11.5
334	CH2+NO<=>OH+HCN	5.07630E-07	10.6
160	HNO+OH=NO+H2O	-4.73016E-07	9.86
335	CH2+NO<=>H+HCNO	-4.67707E-07	9.75
96	NO2+H=NO+OH	4.27484E-07	8.91
341	HCNO+H<=>H+HNCO	3.50842E-07	7.31
365	CH2CO+H=CH3+CO	3.38386E-07	7.05
271	OH+CH2CO<=>HCCO+H2O	-3.28290E-07	6.84
44	CO+OH=CO2+H	2.80683E-07	5.85
346	CH2O+NO2=HCO+HONO	2.55193E-07	5.32

M10 at 300 MPa

	REACTION	SENS COEFF	RELATIVE
333	CH2+NO<=>H+HNCO	3.16923E-06	100.
358	CH2CO(+M)=CH2+CO(+M)	-2.72699E-06	86.0
348	HCO+NO2=H+CO2+NO	2.45420E-06	77.4
19	HNO+NO=N2O+OH	2.32932E-06	73.5
161	H+HNO=H2+NO	-2.17745E-06	68.7
21	HNO+NO2=HONO+NO	-1.42048E-06	44.8
197	HCO+NO=HNO+CO	-1.09563E-06	34.6
23	HONO+OH=H2O+NO2	-7.45269E-07	23.5
166	HNO+HNO=N2O+H2O	7.40861E-07	23.4
192	HNO+NO+NO=HNNO+NO2	7.26328E-07	22.9
364	CH2CO+OH=CH3+CO2	6.71402E-07	21.2
160	HNO+OH=NO+H2O	-6.53846E-07	20.6
226	H+CH2O<=>HCO+H2	-5.75960E-07	18.2
44	CO+OH=CO2+H	5.37203E-07	17.0
341	HCNO+H<=>H+HNCO	4.93591E-07	15.6
186	CO+NO2=NO+CO2	4.91383E-07	15.5
4	NO+OH(+M)=HONO(+M)	4.85394E-07	15.3
193	HNNO+NO=NNH+NO2	4.67402E-07	14.7
258	OH+CH2O<=>HCO+H2O	4.61725E-07	14.6
335	CH2+NO<=>H+HCNO	-3.82736E-07	12.1
271	OH+CH2CO<=>HCCO+H2O	-3.78885E-07	12.0
38	HCO+M=H+CO+M	-3.58735E-07	11.3
50	OH+H2=H2O+H	3.40451E-07	10.7
346	CH2O+NO2=HCO+HONO	3.29461E-07	10.4
181	HNCO+H=NH2+CO	2.99423E-07	9.45
334	CH2+NO<=>OH+HCN	2.50711E-07	7.91
196	HNNO+M=N2+OH+M	2.31203E-07	7.30
149	NH2+NO=N2+H+OH	2.24541E-07	7.09
170	N2O+NO=N2+NO2	2.21935E-07	7.00
365	CH2CO+H=CH3+CO	1.83030E-07	5.78
347	HCO+NO2=CO+HONO	-1.63611E-07	5.16

M10 at 1000 MPa

	REACTION	SENS COEFF	RELATIVE
19	HNO+NO=N2O+OH	5.22508E-06	100.
161	H+HNO=H2+NO	-2.51035E-06	48.0
333	CH2+NO<=>H+HNCO	2.28736E-06	43.8
186	CO+NO2=NO+CO2	1.49803E-06	28.7
358	CH2CO(+M)=CH2+CO(+M)	-1.47604E-06	28.2
96	NO2+H=NO+OH	-9.16731E-07	17.5
21	HNO+NO2=HONO+NO	-8.94653E-07	17.1
348	HCO+NO2=H+CO2+NO	8.64307E-07	16.5
166	HNO+HNO=N2O+H2O	7.51338E-07	14.4
226	H+CH2O<=>HCO+H2	-7.38913E-07	14.1
149	NH2+NO=N2+H+OH	6.78862E-07	13.0
44	CO+OH=CO2+H	6.40842E-07	12.3
160	HNO+OH=NO+H2O	-6.13319E-07	11.7
118	H+HNO=NH+OH	5.68030E-07	10.9
101	NCO+OH=NO+CO+H	5.44861E-07	10.4
50	OH+H2=H2O+H	5.15404E-07	9.86
181	HNCO+H=NH2+CO	4.69344E-07	8.98
362	CH2CO+OH=CH2O+HCO	-4.56085E-07	8.73

3	H+NO(+M)=HNO(+M)	4.55213E-07	8.71
196	HNNO+M=N2+OH+M	4.21638E-07	8.07
341	HCNO+H<=>H+HNCO	3.98903E-07	7.63
363	CH2CO+OH=CH2OH+CO	-3.77101E-07	7.22
364	CH2CO+OH=CH3+CO2	3.04441E-07	5.83
192	HNO+NO+NO=HNNO+NO2	2.85626E-07	5.47

Report Documentation Page

Form Approved
OMB No. 0704-0188

1. REPORT DATE (DD-MM-YYYY)	2. REPORT TYPE	3. DATES COVERED (From - To)
February 2003	Final	October 1999–October 2002

4. TITLE AND SUBTITLE
CYCLOPS, A Breakthrough Code to Predict Solid-Propellant Burning Rates

5a. CONTRACT NUMBER

5b. GRANT NUMBER

5c. PROGRAM ELEMENT NUMBER

6. AUTHOR(S)
Martin S. Miller and William R. Anderson

5d. PROJECT NUMBER
622618.H80

5e. TASK NUMBER

5f. WORK UNIT NUMBER

7. PERFORMING ORGANIZATION NAME(S) AND ADDRESS(ES)
U.S. Army Research Laboratory
AMSRL-WM-BD
Aberdeen Proving Ground, MD 21005-5066

8. PERFORMING ORGANIZATION REPORT NUMBER
ARL-TR-2910

9. SPONSORING/MONITORING AGENCY NAME(S) AND ADDRESS(ES)

10. SPONSOR/MONITOR'S ACRONYM(S)

11. SPONSOR/MONITOR'S REPORT NUMBER(S)

12. DISTRIBUTION/AVAILABILITY STATEMENT
Approved for public release; distribution is unlimited

13. SUPPLEMENTARY NOTES

14. ABSTRACT
Theoretical capability to predict the burning rate of real propellants from their ingredients would be an invaluable aid to formulating new propellants. Despite progress over the last decade on a very few simple ingredients, such as cyclotrimethylenetrinitramine (RDX), and a few simple binary mixtures, no general capability of this sort exists today. This shortcoming is not due to insufficient computational resources, but to a lack of understanding of fundamental combustion mechanisms in the condensed phase and surface/gas interface for typical propellant ingredients and their mixtures. This difficult problem is likely to remain intractable for some time to come. In this report, we demonstrate that our previously published semi-empirical formalism for single ingredients can be successfully extended to treat multi-ingredient propellants. In particular, for purposes of this report, we confine ourselves to nitrate-ester propellants, using M10, M2, M9, and JA2 as examples. However, the method should also be applicable to other classes of homogeneous propellants and even composite propellants where mixing of ingredients in a surface melt layer or sufficiently small particle sizes remove the multi-dimensional character. The method treats the gas-phase processes on the level of elementary reactions and multicomponent transport. A semi-empirical pyrolysis law coupled with informed estimates of the decomposition products of the condensed phase enables us to finesse the absence of knowledge of the detailed processes occurring in the condensed phase and at the burning surface. Results of a computer code, CYCLOPS, based on this approach, show that both the burning rate and flame structure are well predicted for a series of four U. S. Army gun propellants.

15. SUBJECT TERMS
modeling, burning rate, propellants, nitrate ester, double base

16. SECURITY CLASSIFICATION OF:			17. LIMITATION OF ABSTRACT	18. NUMBER OF PAGES	19a. NAME OF RESPONSIBLE PERSON
a. REPORT	b. ABSTRACT	c. THIS PAGE			Martin Miller
UNCLASSIFIED	UNCLASSIFIED	UNCLASSIFIED	UL	68	19b. TELEPHONE NUMBER (Include area code) 410-306-0718

INTENTIONALLY LEFT BLANK.